U.PORTO
FACULDADE DE CIÊNCIAS
UNIVERSIDADE DO PORTO

MSc

2.º
CICLO

FCUP
ICBAS
I2BC
2015

U.PORTO

Structural Characterization of JIP3/4 Leucine Zipper II Recruitment by kinesin1

Fernando Augusto Raio Vilela

FC

U.PORTO
FACULDADE DE CIÊNCIAS
UNIVERSIDADE DO PORTO

U.PORTO
INSTITUTO DE CIÊNCIAS BIOMÉDICAS ABEL SALAZAR
UNIVERSIDADE DO PORTO

I2BC

cnrs

# Structural Characterization of JIP3/4 Leucine Zipper II Recruitment by kinesin1

Fernando Augusto Raio Vilela

Master's Dissertation presented to Faculty of Sciences of the University of Porto, Institute of Biomedical Sciences Abel Salazar of the University of Porto

Biochemistry

2015

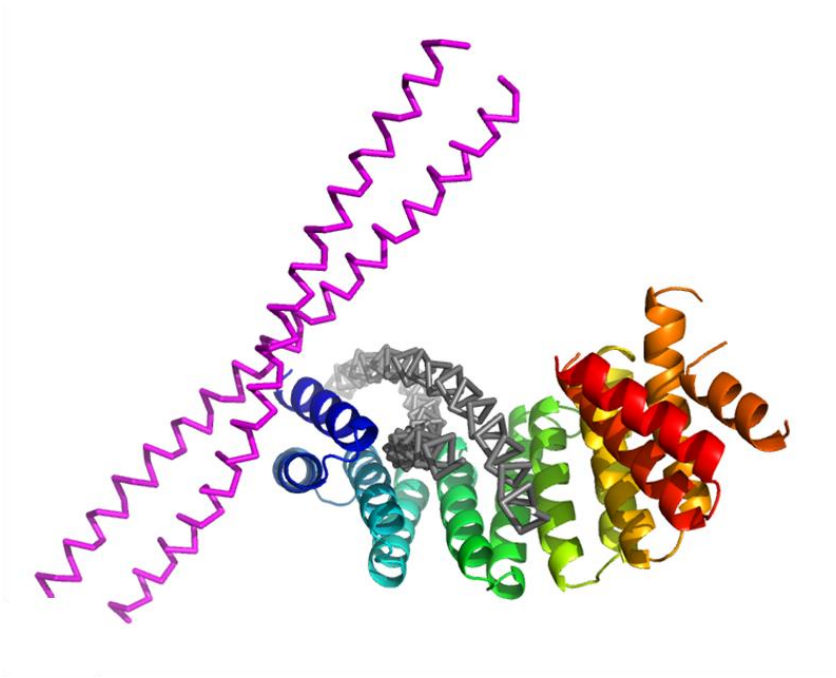

# Structural Characterization of JIP3/4 Leucine Zipper II Recruitment by kinesin1


Fernando Augusto Raio Vilela

Master in Biochemistry

Department of Chemistry and Biochemistry


2015


**Supervised by:**
Julie Ménétrey, Responsable d'Équipe, Institut de Biologie Intégrative de la Cellule
Paola Llinas, Chargée de Recherche, Institut de Biologie Intégrative de la Cellule

Gif-sur-Yvette, Paris

U.PORTO
FACULDADE DE CIÊNCIAS
UNIVERSIDADE DO PORTO

U.PORTO
INSTITUTO DE CIÊNCIAS BIOMÉDICAS ABEL SALAZAR
UNIVERSIDADE DO PORTO

Todas as correções determinadas pelo júri, e só essas, foram efetuadas.

O Presidente do Júri,

Porto, _____/_____/_____

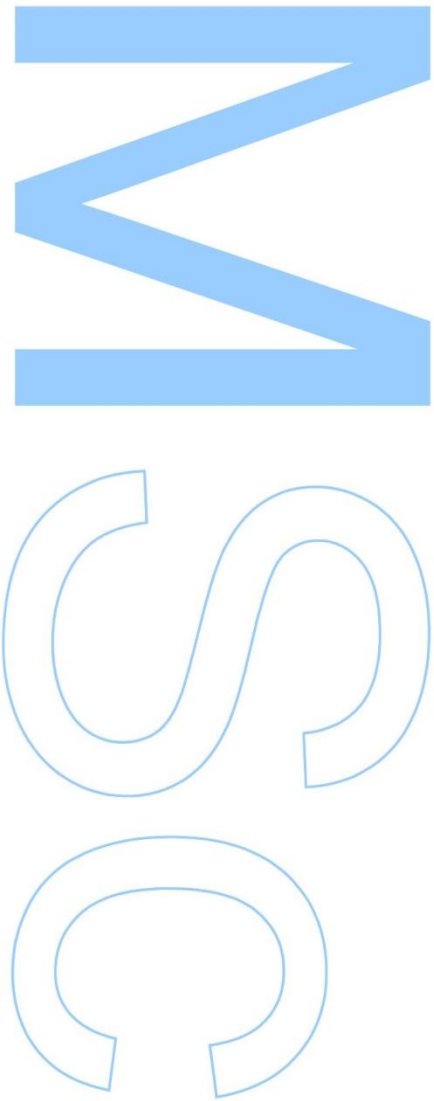

# Acknowledgements

Studying and working in the Life Sciences area has been an incredible opportunity, one that has filled me with an immense sense of happiness and accomplishment throughout the past years. A number of people have been very important in making that possible and supporting me throughout my journey.

Firstly, I would like to thank my family who has given me all the conditions to be successful in my studies. I am very grateful for all the support and love that they have always given me. I would like also to thank my girlfriend, who has given me all the help, support and friendship throughout all these years.

The second year of my master degree was a wonderful experience. I am very thankful to Julie Ménétrey, responsible for our research group, who accepted me to make my master thesis with the group as an Erasmus student. Julie Ménétrey always provided me with the best supervision, knowledge and support from the very beginning. My gratitude also goes to Paola Llinas who accepted me on her project, supervising me and giving me very good opportunities to learn new methodologies on biophysics and biochemistry. Likewise, my gratitude also goes to Mélanie Chenon, for the knowledge which I have acquired from her about on protein production, and for all the time and supervision provided. Julie, Paola and Mélanie, I sincerely thank you for all the support and guidance!

For the very good friendship and partnership in the laboratory, I'd like to thank Quyen Nguyen and Paloma Varela, as well as the rest of the team. In a special way, I'd like to thank all the group for giving me also the possibility to continue my studies and do my PhD. I feel that I will continue to learn a lot from you, and I will give my best to our projects, during the years to come.

It has been an amazing year in Paris. Thus, I'd like to thank all the group and friends of the institute who helped with my integration and have encouraged me to always give my best.

I am also very thankful to the Cité Internationale Universitaire de Paris and to all the friends with whom I shared very good moments. My arrival in Paris would not be possible without the Erasmus+ opportunity provided to my master degree, in my University, which I deeply thank. Likewise, I'd like to thank Elisabete Rodrigues, who helped me with all the preparation for this exchange program.

Before my arrival to the group there were many experiences and knowledges that I took in. Therefore, there are professors and friends that I would like to acknowledge and thank:

- To Professor Sandra Ribeiro, for the opportunities and support she gave me during my bachelor and master degrees.
- To Professor Pedro Fernandes, director of the Master's degree in Biochemistry, as well as all master and bachelor degrees Biochemistry Professors. All contributed to my personal formation, knowledge, and especially to instil in me a curiosity for Science, its developments, its different domains and their bridges. All this has been a great incentive for me to keep on studying and discover more and more.
- To my friends at the IBMC institute, in Porto, who also have given me this ambition to go a step further in Life Sciences.

During my life in Porto there were several organizations I was part of, which highly contributed to my personal development. I am very grateful to: Porto SPRU, Orfeão Universitário do Porto and Núcleo de Estudantes de Bioquímica da Universidade do Porto. Here I made a lot of friends and companions with whom I shared unforgettable experiences that have shaped me as a person.

Finally, a very emotional thank you to the University of Porto and the two Faculties I joined: the Faculty of Sciences and the Institute of Biomedical Sciences Abel Salazar. There are no words to express my gratitude for all these years of learning, curiosity, friendship and adventure.

To all my friends, with whom I've shared countless moments of my life so far, and to the One who I believe always follows us, a warm thank you for everything.

***Virtus Unita Fortius Agit***

# Abstract

In neurons, kinesin1 transports vesicles, protein complexes, as well as various cargo assemblies toward the plus-end of microtubule tracks. This cargoes' transport allows neurons to perform basic physiological functions, as cell's maturation and synaptic transmission. One of the first kinesin1's cargo identified was the JNK-interacting protein 3/4 (JIP3/4) sub-family. Beyond cargoes' functions, these proteins act as scaffolds on JNK and p38 mitogen-activated protein kinase (MAPK) cascades. JIP3/4 are recruited by kinesin1 through a dual binding mode. Here, we aimed to elucidate this characteristic recruitment, by examining one of the interfaces at the molecular level. The objective of this study is the structural characterization of the recruitment of the Leucine Zipper II (LZII) of JIP3/4 by the kinesin light chain 1 (KLC1) of kinesin1. Several advancements were realized.

During this Master's project, KLC1 and JIP3/4 mutants were produced, purified and structurally characterised; this work is not yet fully completed. Identification of JIP3_LZII binding surface was investigated, using alanine scanning on 3 heptad repeat defined accordingly with a docking model. Also, encouraging preliminary studies to determine the low resolution 3D structure by SAXS of the complex were also performed. Future works will be made, aiming to complete the structural characterization of the KLC1-binding surface on JIP3_LZII. New JIP3_LZII mutants have to be produced, their structural integrity checked and their interaction with KLC1 investigated. Finally, the 3D structure of the KLC1:JIP3/4 complex have to be determined by SAXS.

Key words: kinesin1, KLC1, JIP3/4, cargo recruitment, Leucine Zipper, TPR domain, structural characterization, MST, nanoDSF, CD, crystallization.

# Index

# List of Figures and Tables

# Abbreviations

| | |
|---|---|
| Abs | Absorbance |
| BSA | Bovine serum albumin |
| CD | Circular Dichroism |
| CV | Column volume |
| GF | Gel Filtration |
| GFP | Green-Fluorescent protein |
| GST | Glutathione-S-transferase |
| His | Histidine |
| HTX | High Throughput Crystallisation Laboratory |
| IPTG | Isopropyl-B-D-thiogalactopyranoside |
| JBD | JNK-binding domain |
| JIP | JNK-interacting protein |
| KHC | Kinesin high chain |
| KIF | Kinesin family |
| KLC | Kinesin light chain |
| LB | Lysogeny broth |
| LZ | Leucine Zipper |
| MALS | Multi-Angle Light Scattering |
| MAPK | Mitogen-activated protein kinase |
| MST | Microscale Thermophoresis |
| nanoDSF | Nano Differential Scattering Fluorimetry |
| O/N | Overnight |
| OD | Optical Density |
| PAGE | Polyacrylamide gel electrophoresis |
| PBS | Phosphate buffered saline |
| PDB | Protein Data Bank |
| rpm | rotations per minute |
| SAXS | Small-Angle X-ray scattering |
| SDS | Sodium dodecyl sulfate |
| SEC | Size exclusion chromatography |
| SPR | Surface Plasmon Resonance |
| Tm | Melting temperature |
| TPR | Tetratricopeptide repeat |
| TSA | Thermal Shift Assay |

# Introduction

# 1. Molecular Motors

Intracellular communication plays a very important role for cell life (Vale 2003). Inside of an eukaryotic (or prokaryotic) cell, there are structures called cytoskeletal filaments that allow the organization and communication between organelles, vesicles and organic molecules. In fact, beyond their structural functions, cytoskeletal filaments operate as tracks, allowing the traffic of vesicles, organelles, proteins and nucleic acids (Hirokawa 1998). Molecular motors are able to walk along these macromolecular assemblies. At the moment, three super-families of molecular motors have been identified – myosins, dyneins and kinesins (Vale 2003, Hirokawa and Takemura 2005). Myosins bind to actin filaments in order to perform a short-range transport below the plasma membrane and realize muscle contraction (Foth, Goedecke et al. 2006). On their hand, dynein and kinesin proteins perform minus- and plus-end directed transport, along microtubules, but also motility on flagella and cilia (Karki and Holzbaur 1999). Kinesins (also known as KIFs) transport cargoes along microtubules, using chemical energy from ATP hydrolysis in order to produce mechanical energy (conformational changes), leading to protein motion (Hirokawa 1998). Here, we focus on the interaction of kinesins and their cargoes. Indeed, kinesins transport vesicles, mitochondria, multi-protein complexes, synaptic precursors, as well as mRNAs, from a point to another on the cell, where these biological assemblies are requested, allowing different physiological functions (Hirokawa, Noda et al. 2009).

Nowadays, at least 45 mammalian KIF genes have been identified, leading to specificity on different functions and capacities to recruit cargoes. KIF genes have been classified into 14 classes, which represent three major protein groups, where the position of the motor domain is considered. Kinesins' motor domain allows the binding to microtubules and the hydrolysis of ATP. They also contribute to quaternary organization of kinesins (Figure 1) (DeBoer, You et al. 2008).

## 1.1 Kinesin1

Our case in study is kinesin1. This protein is implicated in various biological transport processes, on different cells' types. Kinesin1 is a key on the bidirectional cargoes transport between endoplasmic reticulum and Golgi, Golgi and plasma membrane, as well as on the transports of lysosomes (Lippincott-Schwartz, Cole et al.

1995, Santama, Connie et al. 2004, Woźniak and Allan 2006). Moreover, in neurons, this molecular motor plays main roles on growth, development and transport functions (Hirokawa, Noda et al. 2009). In the axon, kinesin1 guides membrane organelles and protein complexes from the minus-end points of the neuron cell body, along axon microtubule tracks, toward the plus-end terminal on the synaptic region (Bowman, Kamal et al. 2000). Frequently, kinesin1 uses adaptor or scaffold proteins to recruit their cargoes. However, this transport could also exist due to direct binding of kinesin1 to its cargoes (Schnapp 2003). These transport functions on neurons allow their polarization development, neurites elongation, synaptic transmission efficiency, dendrites synaptic plasticity, as well as an active mitochondria distribution and mRNAs transport (Hirokawa, Noda et al. 2009, Hirokawa, Niwa et al. 2010). Kinesin1's dysfunction on cargoes transport in neurons contributes to several diseases, as Parkinson, Hereditary spastic paraplegia, Ciliopathies and Alzheimer. (Gunawardena and Goldstein 2001, De Vos, Grierson et al. 2008, Gerdes, Davis et al. 2009).

Kinesin1 has a heterotetrameric quaternary organization with two kinesin heavy chains (KHC) and two kinesin light chains (KLC). Several domains have been implicated in cargo binding, especially the C-terminal regions of KHC and KLC chains (Adio, Reth et al. 2006, Gindhart 2006). Each KHC has (a) the N-terminal motor with ATP hydrolysis activity and microtubule binding, (b) a coiled-coil stalk domain, providing the ability for a successful dimerization and mechanical mobility, and (c) a tail domain, as a protein interacting region of the heavy chain, leading an important role on cargoes recruitment. KLC chains possess two different parts: (i) an alpha-helix coiled-coil domain on N-terminal, which binds KHC stalk region and (ii) a TPR (tetratricopeptide repeats) domain in their C-terminal (Figure 1) (DeBoer, You et al. 2008). In KLC's case, the TPR domain is arranged as six TPR motifs in tandem involved in protein-protein interactions (Zhu, Lee et al. 2012). Indeed, the TPR domain of KLC is involved in cargo recruitment (Hammond, Griffin et al. 2008) (Verhey, Meyer et al. 2001).

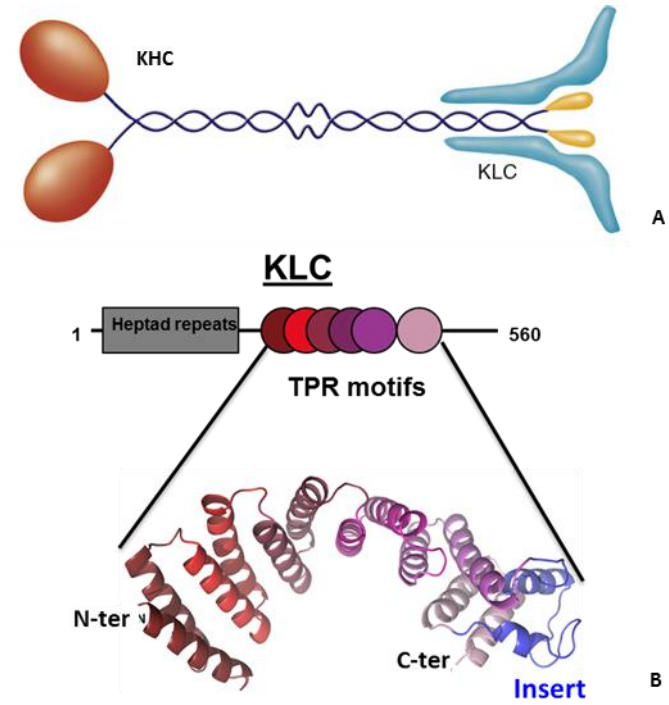


Figure 1 – A - Kinesin1. KHC chains: on red – motor domains; on blue line – stalk regions; on yellow – tail domains. KLC chains are highlighted on light blue. Adapted from (Hirokawa, Niwa et al. 2010). B – Schematic representation of KLC domains: N-terminal heptad repeat and the 6 TPR motifs, positioned on C-terminal of KLC.

During the last years, the motor domain of kinesin1 has been well characterized (Kaan, Hackney et al. 2011). However, less is understood about cargoes recruitment and recognition by C-terminals of KLC and KHC domains. The goal of this study is to understand, in a structural point of view, how kinesin1 recruits their cargoes.

## 2. JNK-Interacting Protein (JIP) Family

JNK-Interacting Proteins (JIP) are scaffold proteins, which co-localize signalling module components, controlling cellular processes including differentiation, growth, immune response and apoptosis. Precisely, JIPs have these functions on JNK and p38 mitogen-activated protein kinase (MAPK) cascades (Morrison and Davis 2003). These signalling pathways are evolutionarily conserved on cells and, in mammals, two JIP sub-families were described (JIP1/JIP2 and JIP3/JIP4) (Yasuda, Whitmarsh et al. 1999). All JIPs are found in the cytoplasm of the cells, but also nuclear localization has been observed. JIP family possesses a considerable domains' diversity, allowing also the regulation of other cell's functions (Whitmarsh 2006). In neurons, JIPs act also in

the regulation of axonal vesicle transport, via adaptor proteins for anterograde and retrograde transport on axons. JIP3 and JIP4 are structurally distinct from JIP1 and JIP2, apart from their JNK-binding domain (Kelkar, Standen et al. 2005). Here, we will discuss the sub-family JIP3 and JIP4, targets of our study.

## 2.1. JNK-interacting Proteins 3 and 4 (JIP3 and 4)

JIP3 and JIP4 have high homologous multi-domain protein sequences. On their N-terminus, these proteins possess two distinguished Leucine Zipper (LZ) domains, I and II, as well as a JNK-binding domain (JBD). On the C-terminus, a conserved domain is present (Figure 2). These proteins have particular expression patterns on tissues. JIP4 is ubiquitously expressed in cells and JIP3 is highly expressed on neurons (Whitmarsh 2006). Interestingly, JIP3 plays crucial roles in these cells, not only as adaptor proteins for kinesins and dyneins' recruitment, on anterograde and retrograde axonal transport, respectively, but also as signalling cascade transporters, guided by molecular motors along the axon (Kelkar, Gupta et al. 2000). Physiologically, JIP3 and JIP4 participate on axonal vesicle transport, axonal elongation and neuron regeneration, nerve injury signalling and neuronal apoptosis pathways. (Verhey, Meyer et al. 2001, Nguyen, Lee et al. 2005) (Cavalli, Kujala et al. 2005). In fact, JIP3/4 were one of the first identified protein cargoes of kinesin1 (Verhey, Meyer et al. 2001).


Figure 2 - Schematic representation of JIP3, *Homo sapiens*. LZ - Leucine Zipper.

## 3. JIP3/4 recruitment by kinesin1

In neurons, JIP3/4 are recruited by kinesin1 through a dual binding mode. During recent past, two different and independent interaction interfaces between JIP3/4 and kinesin1 have been identified. On the one hand, the tail domain from kinesin1 KHC chain directly binds to the Leucine zipper I (LZI) of JIP3/4 (Watt, Dixit et al. 2015). This KHC_tail:JIP3/4_LZI interface is not developed in this manuscript. On the other hand, the TPR domain of KLC directly interacts with the Leucine Zipper II (LZII) of JIP3/4 (Nguyen, Lee et al. 2005, Hammond, Griffin et al. 2008). Together, these two interactions regulate this cargoes recruitment pathway in neurons, as well as kinesin1 and JIPs' functions on these cells. Independent binding interfaces co-exist, being predicted that the existence of both interfaces allows a higher specificity of the protein recruitment in case (Watt, Dixit et al. 2015).

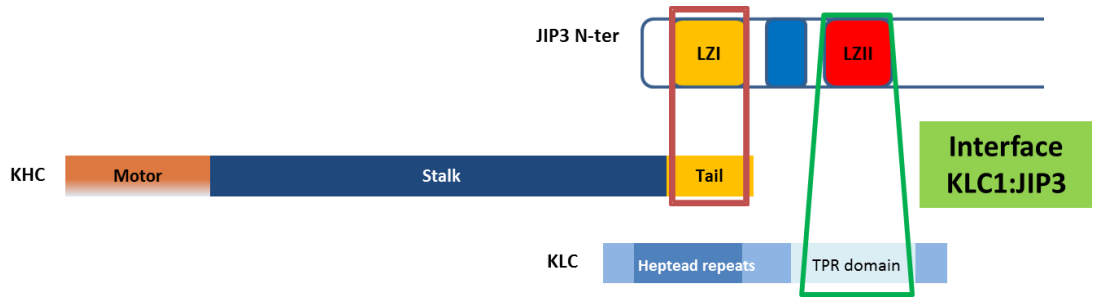


Figure 3 - Schematic representation of the dual binding mode between kinesin1 and JIP3 isoform. KHC_tail: JIP3_LZI interface is highlighted by a red square. Highlighted on green, KLC1_TPR:JIP3_LZII interface, the case in study on this project.

Here, we aim to structurally characterize the JIP3/4_LZII recruitment by TPR domain of KLC1 of kinesin1 (Figure 3, on green). Which residues are involved in each domain of the complex interface, on KLC1 and on JIP3_LZII? How is the 3D structure of the complex? These are questions that we will try to elucidate.

## 4. Previous experiments on the project.

This project has been started by the group before my arrival. In order to structurally characterize KLC1_TPR:JIP3/4_LZII interface, they aim to obtain the 3D structure of the complex by X-ray Crystallography, as well as molecular information on the interaction using biophysical approaches. The group has realized a huge effort in

order to crystallize KLC1:JIP3/4 complex; unfortunately, without success. However, they gained several interesting information on the interaction using biophysical approaches. In other word, they narrowed down the KLC1-interface region, as well as the JIP3/4-interface region.

Altogether, these information allow to propose a docking model of the complex (collaboration with Raphaël Guérois, I2BC). To perform it, we used the 3D structure of KLC1 (PDB entry: 3NF1) and a model of JIP3_LZII computed from the 3D structure of JIP4_LZII (PDB entry: 2W83) (Isabet, Montagnac et al. 2009, Zhu, Lee et al. 2012). Of note, the LZII from JIP3 and JIP4 share high homology (Figure 4). Two different docking models were computed and thus two distinct interfaces were identified (purple and grey chains, Figure 5) for the complex.

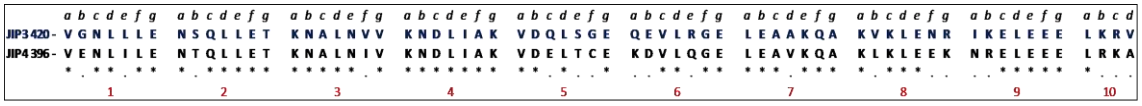


Figure 4 - Sequence alignment of LZII domain from JIP3 and its homologous JIP4. On the first line, coiled-coil heptad organization. Ten heptad repeats are represented. * - same residue; . - no similarity on the residue position.

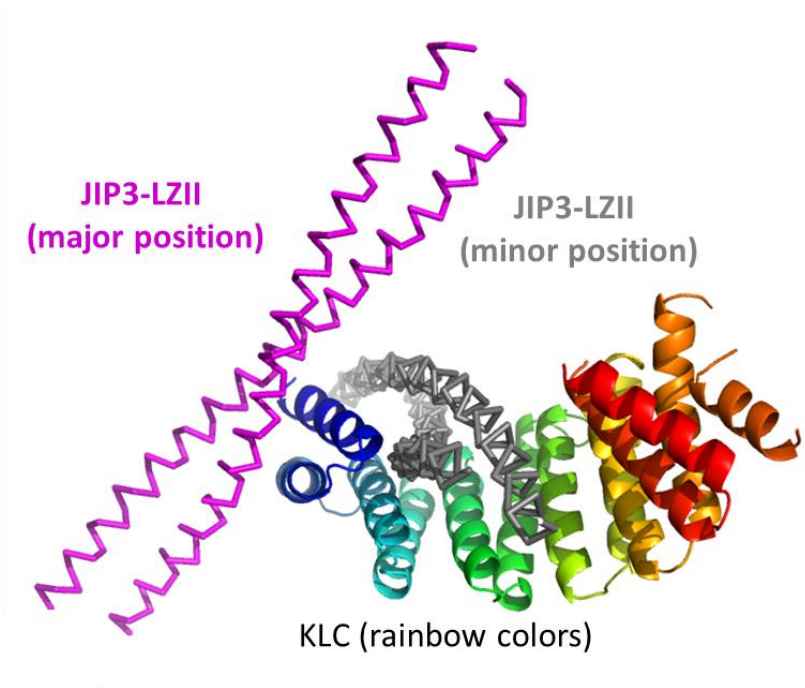


Figure 5 - Docking models for KLC1:JIP3_LZII. Interface 1 (purple) – major position defined; interface 2 (grey) – minor position defined.

Then, my supervisors have realized site directed mutagenesis and affinity binding experiments, using KLC1 and JIP3_LZII fragments, aiming to validate one of the complex interfaces identified by molecular docking. Thus, the first phase of this project was to conceive and produce KLC1 mutants and to perform binding experiments with JIP3_LZII wild type. Several KLC1 mutants were designed, with mutation on residues from the interface 1 (JIP3 in pink, major position - Figure 5) and mutation on residues from the interface 2 (JIP3 in grey, minor position, Figure 5). Binding experiments using Surface Plasmon Resonance (SPR) and Microscale Thermophoresis (MST) clearly revealed that KLC1 mutations on the minor interface (JIP3 in grey) do not prevent interaction with JIP3, while KLC1 mutations on the major interface (JIP3 in pink) prevent the interaction with JIP3. These results confirmed that the JIP3_LZII major position is a good docking model.

The group aimed also to confirm the JIP3_LZII region which interacts with the KLC1_TPR domain using site directed mutagenesis and binding experiments (Phase 2). To make it, several JIP3_LZII mutants were conceived. Leucine zipper motif, as coiled-coil, possesses a seven residues' pattern repetition. Each heptad repeat has seven possible residue positions, named as *a* through *g*, where *a* and *d* are generally hydrophobic residues (Lupas, Van Dyke et al. 1991). Therefore, JIP3_LZII mutants were carefully designed because hydrophobic positions could not be mutated, in order to maintain the structural integrity of the Leucine Zipper domain. According with the molecular docking results, LZII region (predicted as interacting JIP3 surface) has to be tested. So, several JIP3_LZII mutation constructs were designed on the second, third and fourth heptad repeats, on strategic hydrophilic residues. In other words, an alanine scanning has been realized, in order to identify which JIP3_LZII residues are crucial for the complex interaction. Also a charge reversion on one putative salt bridge interaction between KLC1 and JIP3_LZII was conceived. Such an experiment would not only validate the interface, but also identify precisely a salt bridge interaction. Supposing this fact, this charge reversion on both residues would maintain the overall electrostatic forces of the complex interface, maintaining, theoretically, the complex formed.

## 5. My Master Project

In collaboration and with the supervision of the team, I have contributed to the Phase 2 of this project by optimising the expression and purification of KLC1 fragments and JIP3_LZII mutants. Also, I have participated on their structural characterization, by limited proteolysis, Size exclusion chromatography-Multi Angle Light Scattering (SEC-MALS), Thermal Shift Assay (TSA), nano Differential Scattering Fluorimetry (nanoDSF) and Circular Dichroism (CD). I contributed also on KLC1:JIP3/4_LZII complex characterization, by performing preliminary studies using Microscale Thermophoresis (MST). Finally, I have performed JIP3_LZII mutants crystallization trials using the HTX platform, in Grenoble, France, finding several crystallization conditions. Besides, I found new crystallization conditions for a new KLC1 fragment, to be used on the team's work.

Overall, KLC1 fragments and JIP3_LZII mutants were successfully produced, with optimised protocols. Protein characterization was not yet fully completed, but several experiments and optimizations were made, with very positive advancements. In collaboration with the team, I helped also to characterize KLC1:JIP3_LZII interaction and the finalization of Phase 2 of the project will be performed in the near future, using experiments' optimisations here described.

Finally, to further confirm the docking model of the KLC1:JIP3/4_LZII complex, we aim to determine the 3D structure of the complex, at low resolution, using SAXS.

# Materials and Methods

## Transformation

In order to realize protein expression on bacterial systems, *E. coli* strains BL21(DE3)GOLD and Rosetta were transformed with KLC1 and JIP3_LZII mutant constructs previously conceived. After thawing 100 uL of competent cells (prepared accordingly with $CaCl_2$ protocol, not shown), 40 ng expression vectors were added and mix was maintained on ice for 10 minutes. Thus, transformation by heat shock was made at 42°C, during 45 seconds. Afterwards, incubation on ice was performed during 2 minutes. To recover transformed cells, 900 uL of new Lysogeny broth (LB) medium was added and an incubation of 30 minutes was made, at 37°C and 200 rotations per minute (rpm). Finally, 200 uL of culture were placed on LB-agar plates with antibiotic (50 ul/mL of kanamicin or 100 uL/mL of ampicillin, according with antibiotic resistance of expression vectors used). Cells were grown on agar-plates overnight (O/N) at 37°C.

## Protein Expression Tests

After transformation, a bacterial colony was picked up into 2 mL of LB medium within same antibiotic conditions, appropriately to antibiotic resistance of each protein vector. Cells were left by 3 hours at 37°C and 200 rpm. Therefore, culture was transferred to 50 mL of LB medium + antibiotic and incubation O/N was made at same temperature and rotation speed. Concerning induction conditions, a culture dilution was carried out to an Optical Density at 600 nm ($OD_{600}$) of 0.2. Then, cells were incubated in order to reach the growth of $OD_{600}$=0.6, at 37°C. Induction was made with 0.3 mM of Isopropyl-B-D-thiogalactopyranoside (IPTG). Protein expression tests were performed, evaluating three different induction temperatures. Incubation was performed at 30°C and 37°C, independently, during 4 hours, but also at 20°C O/N, all within agitation of 180 rpm. For JIP3_LZII wild type construct, tests were performed with and without the presence of 1% ethanol, in order to induce stress conditions and bacterial response on protein expression. At the end, expression conditions were analysed using Sodium dodecyl sulphate polyacrylamide gels (SDS-PAGE) and Western Blot. Each protein sample quantity deposed was 0.1 of the absorbance unit (correspondent to 1: value of $OD_{600}$ after induction time).

## SDS-PAGE

Gels are composed by two distinct parts: a concentration gel (stacking) and a separation gel (running). Firstly, loading buffer (Annexe 1) was added to each protein fraction in the ratio of 1:5; then, protein was denatured at 95°C during 5-10 minutes. After, samples performed were loaded into gels, in presence of a protein marker as molecular weight control (Page Ruler Prestained Protein Ladder, Thermo Scientific). After migration, gels were stained with Instant Blue (expendeon) and washed with $H_2O$. The composition of SDS gels (stacking and running) is shown on Annexe 2.

## Western Blot

Samples' migration was performed by SDS-PAGE and proteins were transferred onto a cellulose membrane at 250 mA, by 1 hour, merged on transferring buffer (SDS Running buffer with 20% Ethanol). Aiming the protein transfer confirmation, membrane was coloured with Ponceau buffer (0.2% (w/v) of Ponceau and 10% acetic acid – red ponceau staining) and membrane was compared with the results of similar deposition on a blue stained SDS-PAGE. Therefore, blockage was made by submerging the membrane in Phosphate buffered saline x1 (PBS, Sigma), 0.1% of Tween 20 and 5% (w/v) of Nonfat-Dried Milk bovine (Sigma), kindly agitated during 30 minutes at room temperature. Then, cellulose membrane was incubated with GST- or His-tag antibody (anti-GST peroxidase conjugate, Sigma; or Anti-$His_6$ Peroxidase (2), Roche) added to new blockage buffer, on the antibody/buffer volumes' ratio of 1/200 and 1/3000, respectively. Incubation at room temperature was performed, during 1 hour, with slow agitation. Consequently, membrane wash was made in three times of 10 minutes, using PBS x1 and 0.1% of Tween 20. In order to obtain chemoluminescence detection, both GST- and His-tag antibodies possess a signalling domain of peroxidase activity. Substrate was prepared using Super Signal West Pico Chemoluminescence Substrate (Thermo Scientific) and 1 mL of it was overspread on the membrane. After an incubation of 3 minutes, chemoluminescence was measured by FujiLas-3000 equipment, performing high sensitivity and an exposure time between 10 seconds and 1 minute, depending on the chemoluminescence signal.

## Glycerol Stocks

Concerning the cryopreservation of transformed cells for future works, pre-cultures from protein expression tests were used to make glycerol stocks. After mixing, we achieved glycerol's final concentration of 40% and cells could be frozen on liquid nitrogen and stored at -80°C.

## Solubility and Minipurification Tests

Here, we aimed to select the protein expression conditions that allow the higher production of soluble protein, but also to qualitatively evaluate its purification yield.

For solubility tests, lysis was performed with pellets collected from expression tests. Lysis buffers used (Annexe 3) were enriched with 0,1% Triton, 1mM PMSF, 2 ug/mL of leupeptin and aprotinin, 0.7 mg/mL of lysozyme, 10 units/mL of benzonase and 1mM DTT. The buffer volume/pellet ratio performed was 1 mL per pellet from 5 mL culture. Afterwards, mild agitation was performed during 1 hour at 4°C, and by centrifugation, soluble and insoluble fractions were separated (using a Centrifuge 5415R, eppendorf), at 16000g and same temperature, by 30 minutes. With the aim of comparing different conditions, equal quantities were deposed on SDS-PAGEs and fractions with higher protein solubility were selected for purification tests.

In the interest of performing minipurification tests, 200 uL of His- or GST-tag resins (Ni-NTA Agarose, Qiagen, and Glutathione Sepharose 4 Fast Flow, GE Healthcare, respectively) were washed with, firstly, 2 mL of $H_2O$, and secondly 2 mL of correspondent lysis buffer (Annexe 3), by centrifugation at 400 rpm, during 5 minutes. Resins were used according with tagged-proteins in study. Then, 2 mL of soluble fractions were added to resins and mild constant inversion of samples was made at 4°C, by 1 hour. After similar centrifugation, not retained fractions were collected. Resins' wash were made using 600 uL of wash buffer (Annexe 3) and centrifuged (at the same conditions), by 3 times. Finally, 100 uL of elution buffer (with high concentration of imidazole or reduced-glutathione, depending on the protein-tag, Annexe 3) was added and new centrifugation was realized, eluting the protein of interest from resins. Samples from all steps were analysed by SDS-PAGE and purification yield was qualitatively evaluated for each case.

## Protein Expression at high scale

For large scale protein expression, pre-cultures were grown in LB medium O/N for each protein, with proper antibiotic conditions. Thus, cell growth and $OD_{600}$ required conditions were performed, accordingly with expression tests' results for each protein, into the final volume of 1L of YT medium. Induction conditions previously chosen for each protein were consequently used, as described on Results. Hence, cell cultures were centrifuged at 4000 rpm and 4°C, during 30 minutes, by a JLA-8.1000 rotor on a centrifuge Avanti J-26 XP (Beckman Coulter). Finally, pellets were resuspended on PBS x1 buffer, centrifuged again (on a Centrifuge 5330R, eppendorf) at 4000 rpm, by 20 minutes, and pellets were stored at -20°C or directly used for protein purification.

## Protein Purification

Aiming the purification of the proteins in study, different approaches were performed, taking in consideration that KLC1s are His-tagged and JIP3_LZIIs are GST-tagged. Firstly, an extraction and clarification step was carried out, concerning the separation of soluble and insoluble proteins, as well as other bacterial components, also insoluble. For that, bacterial lysis was made, using lysis buffer (dependent on each protein; Annexe 4) to the final volume of 50 mL/pellet of 1L culture. Lysis buffers were enriched by 0,1% Triton, 1mM PMSF, protease inhibitors leupeptin and aprotinin at the concentration of 2 ug/mL, 0,7 mg/mL of lysozyme, 10 units/mL of benzonase (Sigma) and 1mM DTT. After 1 hour of mild agitation at 4°C, lysate was sonicated in order to have a good lysis yield. Subsequently, a centrifugation was performed at 40000 rpm, 4°C and during 45 minutes, with a TI-70 rotor, working within an Avanti J-26 XP (Beckman Coulter), leading to lysate clarification. Secondly, a capture step was made using the soluble fraction, in order to isolate and concentrate the protein of interest, by using Protein Affinity Chromatography. Depending on the purified protein, we performed different strategies. The followed protocols were realized to purify KLC1 and JIP3_LZII fragments. To manage all processes, an AKTA Purifier or an AKTA Pure system (GE Healthcare) were adopted, at 10°C.

### *KLC1 fragments*

KLC1s allowed their purification by His-tag Affinity Chromatography, separating the majority of the contaminants from the protein fragments in consideration. On the second step, a size exclusion chromatography was always performed, leading to protein polishing and an higher yield of purification, in terms of protein sample homogeneity, oligomerization state and contaminants elimination.

Previously, a 5 mL Histrap Column HP (GE Healthcare) was equilibrated with 5 column volumes (CV) of lysis buffer (Annexe 4). After loading the column with the soluble fraction (at 1 mL/min and a maximum of 0.3 MPa pressure), a wash was performed with 5 CV, using wash buffer (Annexe 4). Then, elution was performed by imidazole gradient concentration, using wash and elution buffers (Annexe 4). We realized an imidazole gradient of 20 mM to 500 mM, during 5 CV, at same elution debit. Fractions were collected and analysed by SDS-PAGE. Therefore, we made a protein fractions selection to be concentrated (volume around 6 mL) and injected on a Size Exclusion Chromatography (SEC), for further purification.

Then, a HiLoad 16/60 Superdex 75 prep grade (GE Healthcare) was used to perform the polishing step for KLC1s. Column was previously equilibrated with 2 CV of KLC1 storage buffer (Annexe 4). Elution was made at 0.8 mL/min and a maximum of 0.5 MPa system pressure. Fractions were collected and analysed by SDS-PAGE. Then, we selected KLC1 protein fractions to store on batches, considering the yield of purification. Protein concentration was determined by Abs 280 nm. Purified KLC1s were also analysed on a SDS-PAGE batch and frozen within liquid nitrogen for storage.

### *JIP3_LZII wild type and mutants*

Several strategies were conceived and tried; afterwards, a strategy of 5 purification steps was optimised and applied to all JIP3_LZII mutants.

(a) GST-tag protein affinity chromatography

Firstly, a GST-tag affinity chromatography was performed in order to separate our GST-protein target from the other biological molecules, present in the bacterial soluble lysate. A 5 mL GST-trap FF (GE Healthcare) column was equilibrated with 5 CV of lysis buffer (Annexe 4). After loading the column with the soluble fraction (at 1 mL/min and a maximum of 0.3 MPa pressure), a wash step was performed with 5 CV, using wash buffer (Annexe 4). Therefore, elution was made using elution buffer,

containing 10 mM of reduced glutathione (Annexe 4). Fractions were analysed by SDS-PAGE and then selected for GST-cleavage O/N.

(b) JIP3_LZII-GST cleavage O/N, using rTEV

Protein concentration was measured by Bradford Method and rTEV His-tagged was added in the ratio of 1:20. rTEV used was produced by the team (protocols not mentioned on this manuscript). Incubation was performed at 10ºC O/N, with slow agitation. Samples of rTEV, JIP3_LZII GST-tagged, as well as initial and final incubation moments were analysed by SDS-PAGE.

(c) His-tagged protein contaminants elimination

After GST- cleavage, we aimed to eliminate rTEV-His-tagged and other possible His-protein contaminants of the incubated protein mix. Then, a 5 mL His-trap Column HP (GE Healthcare) was equilibrated by 5 CV of His-buffer A (Annexe 4) and column was charged with the protein mixture (at 1 mL/min and a maximum of 0.3 MPa pressure). Flow through was collected and protein fractions were selected to be analysed by SDS-PAGE. Afterwards, elution of protein contaminants was performed from the column, using His-Buffer B (Annexe 4), and consequently eliminated.

(d) GST-tagged protein contaminants elimination

By the same strategy of (c), we aimed to exclude all GST-protein contaminants from the selected fractions of previous step. So, we used a 5 mL GST-trap FF (GE Healthcare) column to realize it. After equilibrated with GST-buffer A (Annexe 4), column was charged (at 0.5 mL/min and a maximum of 0.3 MPa system pressure) with the previous selected protein fraction and flow through was recovered. New protein fractions were selected to be analysed by SDS-PAGE. GST-protein contaminants were eluted and consequently eliminated, using GTS-Buffer B (Annexe 4). Recovered JIP3_LZII fractions were concentrated, using Amicon Cut off 3kDa falcons (Millipore), to a volume around 6 mL, in order to be injected on a gel filtration column, for further purification.

(e) Size Exclusion Chromatography (SEC)

Finally, a HiLoad 16/60 Superdex 75 prep grade (GE Healthcare) was used to perform the last purification step of JIP3_LZII fragments. Column was previously equilibrated with 2 CV of JIP3_LZII storage buffer (Annexe 4). Elution was made at 0.8 mL/min and a maximum of 0.5 MPa system pressure. Fractions were collected and analysed by SDS-PAGE gel. Then, we selected for storage JIP3_LZII protein fractions,

considering the yield of purification. Protein concentration was measured by Abs 280 nm. After, fractions were concentrated using Amicon Cut off 3kDa falcons (Millipore). JIP3s_LZII were analysed by SDS-PAGE batch and frozen within liquid nitrogen for storage at -80ºC.

## Bradford Method

In order to measure each protein concentration by Bradford, two samples with different protein dilutions were prepared. For the first sample, protein was diluted with its storage buffer at 1:20 and 20 uL were added to 1 mL of Bradford reagent (Quick Start Bradford 1x Dye Reagent, Bio-Rad). For the second one, protein was diluted with storage buffer at 1:50 and 20 uL were added at the same manner. To make the control, 1 mL of Bradford reagent was mixed with 20 uL of storage buffer. After vortex mixing, incubation during 5 minutes was made in the dark. Absorbance was measured at 595 nm and concentration values were obtained due to a linear regression made with Bovine serum albumin (BSA - Quick Start Bovine Serum Albumin 2 mg/mL, Bio-Rad), measuring quantities already known, from where the linear equation was obtained: Abs = 1.036C, with $R^2$=0,96763 (Abs - absorbance, C - concentration).

## Limited proteolysis

In this methodology, KLC1s were incubated, separately, with 9 different proteases: trypsin, alpha-chemo-trypsin, elastase, papain, subtilisin, endoproteinase glutamine-C, thrombin, proteinase K and rTEV. We aim to have evidences if the protein in study is well folded. Initially, studied proteins were diluted to 0.1 mg/mL. Respective concentrations were converted to Molar units and all proteases used were incubated with target proteins in the molar ratio of 1:500. To realize t=0 conditions for each KLC1 fragment tested, 20 uL of diluted protein were denatured to be analysed by SDS-PAGE. Afterwards, nine independent incubations were performed in eppendorf tubes, for each KLC1. On each tube, we used 100 uL of KLC1 fragment in case and proper quantity of each protease is added, according with the mentioned ratio. Then, we mixed and incubated at room temperature. Finally, different incubation moments were analysed: at 5, 10, 20 and 30 minutes, taking 20 uL from each incubation tube, to be denatured and analysed by SDS-PAGE.

## Thermal Shift Assay (TSA)

For TSA experiments, KLC1 fragments were tested on different buffer conditions (Annexe 5) aiming the knowledge of KLC1s' melting temperatures and folding on different buffer, pH and salt conditions. To realize it, we used VWR-Axygen PCR microplates and, to cover them, Optical adhesive Covers (Applied Biosystems). Initially, KLC1 fragments were diluted into 0.5 mg/mL. Then, 24 uL of each buffer condition were putted on each well and mixed with 3 uL of diluted KLC1. Therefore, 3 uL of Sypro Orange 5x (Sigma-Aldrich) were added to each condition tested and plates were covered. Experiments were performed in triplicate, in order to validate the achieved results. Measurements were made on an iCycler iQ5 Real-Time PCR (Bio-Rad), with excitation wavelength of 548 nm and emission wavelength of 595 nm, between 20ºC and 90ºC, with increments of 0.5ºC.

## Nano Differential Scattering Fluorimetry (nanoDSF)

Experiments were performed on a Nanotemper Technologies Workshop, organised by the group, and on the Structure, Design & Informatics Department of Sanofi Aventis, Vitry-sur-Seine, Paris, where time for experiments on a Prometheus NT.48 were kindly provided.

Initially, we used JIP3_LZII_#10 in order to know if it is possible to define a melting temperature to JIP3_LZII mutants, which contain on their N-terminal two tryptophan residues, capable of being followed by this methodology. Thus, we concentrated JIP3_LZII_#10 to 1.5 mg/mL. Protein dilutions in the ratio of 1:5 were realized, using a standard screening buffer (Annexe 6). Diluted proteins were loaded on High Sensitivity capillaries and analysed by nanoDSF. Fluorescence 330 nm and 350 nm measures were performed between 20ºC and 95ºC.

After confirming the possibility of following the denaturation state of JIP3_LZII mutants by nanoDSF, experiments were also performed (not yet validated by triplicate measures) for all JIP3/4_LZII fragments and mutants in study. We performed similar dilutions to test different buffers, used on SPR, CD and gel filtration protocols by the group. We also tested the effect of refreeze and thaw on proteins, within gel filtration buffer. Same capillaries and nanoDSF measures were performed (Annexe 6).

## Size Exclusion Chromatography - Multi-Angle Light Scattering (SEC-MALS) - performed on Macromolecular Interaction Platform (PIM, Gif-sur-Yvette)

Protocols are not extensively explained in this manuscript. I gave my contribution on experiments' preparation and analysis. I did not perform directly MALS protocols for JIP3_LZII and KLC1 fragments. However, main guidelines are explained. For KLC1 fragments, a Superdex 200 10/300GL increase was used, with debit 0.5 mL/min of 50 mM Hepes pH 8.0 and 200 mM NaCl. The volume of 100 uL was injected on the column, at the concentration of 2 mg/mL. For JIP3_LZII fragments, optimizations are currently in progress.

## Circular Dichroism (CD)

Firstly, in order to eliminate chloride ions (from NaCl and Tris) from JIP3_LZII storage buffers, dialysis was made to change buffer conditions into 20 mM phosphate pH 7.0, 150 mM NaF and 0.05% Tween 20. Afterwards, we concentrated all JIP3_LZII mutants to the range of 0.5 mg/mL. CD experiments were performed on a J-810 Spectropolarimeter (Jasco Inc.), using a circular cuvette with 100 um of optic trajectory. We performed all measures between 180 nm and 260 nm, continuously, with a scanning speed of 50-100 nm/min, at room temperature. Concerning the calculation of protein secondary structure prediction percentages for JIP3_LZII mutants, an average was calculated with CDSSTR (theoretical database software chosen for the case in study) results, based on two basis set options (SDP42 and SDP48), chosen accordingly with the theoretical prediction of JIP3_LZII structure.

## Microscale Thermophoresis (MST) – preliminary studies

Protein interaction assays were performed, by MST, using JIP4_LZII_#1 and KLC1_#0. Experiments were realized on a Monolight NT. 115 Instrument (Nanotemper Technologies). KLC1 was labelled with kit MO-L002 Monolight Protein Labeling Kit Green-NHS (amine reactive, Nanotemper Technologies), maintaining its buffer, accordingly with manufacturers protocols. In the final, fractions of labelled protein were collected and concentrations were determined by Abs 280 nm. The more concentrated KLC-labelled fraction was diluted and used on KLC1:JIP4_LZII MST assays at the

initial concentration of 1,5x10-7 M (in 50 mM HEPES pH 7.0, 350 mM NaCl, 0.05% Tween 20 and 5 mM MgCl2). Non-labeled protein, JIP4_LZII, was used at the initial concentration of 715000 nM (in 50 mM Hepes pH 7, 50 mM NaCl, 5 mM MgCl2, 0.06% LDAO, 1 mM DTT) and sixteen dilutions were realized, according with Nanotemper protocols. Measures were performed using 40% MST Power and 90% LED Power, also with standard MST program parameters.

## Crystallization trials of JIP3_LZII wild type and mutants - High Throughput Crystallisation Laboratory - (HTX)

All JIP3_LZII mutants were concentrated in the order of 1 mg/mL, frozen, and sent to High Throughput Crystallisation Laboratory - (HTX), Grenoble, France. Each mutant was tested by vapour diffusion sitting drop. We requested sitting drop crystallization assays for each mutant in two different temperatures, 4ºC and 20ºC, as well as in two different crystallization screening kits: Classical Suit (Qiagen) and Grid Screen Salt (Hampton Research). Methods are not extensively described, due to their execution by HTX collaborators. HTX gives to users the possibility of following all assays due to pictures which are taken periodically, being accessible on the user profile of the website https://embl.fr/htxlab/index.php. High resolution scope is available.

## Crystallization trials of new KLC1 fragments

3D structure of KLC1 TPR domain is already published. However, we performed crystallization trials to new KLC1 fragments (KLC_#1, Annexe 7) aiming the achievement of new crystallization conditions of the protein, to be used by the laboratory, in the course of other projects. Here, it was always realized vapour diffusion hanging drop methodologies, performed in the lab, without robotic technology. Initially, we performed crystallization trials (1uL protein + 1 uL precipitant condition - drop; 500 uL reservoir – 24 wells plate) with a Solubility Screening (Annexe 8), in order to know the range of protein concentration that could be used, but also favourable pH and salt conditions for crystallization. Afterwards, crystallization trials were performed using two different crystallization screening kits: Classical Suit and Ammonium Sulphate ($AMSO_4$) Suite Screens (Qiagen). On hanging drop 48 wells plates, we mix 1 uL protein+ 1 uL precipitant condition on drops and 200 uL of same condition on reservoir wells. All

plates were conserved at 17ºC. After two weeks incubation, promising conditions were selected (shown on Results). Methylene Blue Solution (IZIT Crystal Dye, Hampton Research) was used on the main crystal condition found, aiming the confirmation of protein crystals' formation. Optimisations are currently in course.

# Results

# Protein Production

## KLC1 fragments

### Expression Conditions Optimisation

**Protein expression tests** - Protein expression conditions were optimized for KLC1 constructs and high scale protein production was performed. Figure 6 shows that KLC1_#1 (Table 1) is well expressed in *E. coli* Rosetta. For the remaining KLC1 constructs (Table 1), the results of expression tests were similar (not shown). In the case of KLC1_#1 construct, two *E. coli* Rosetta conditions were tested to realize solubility and minipurification assays: (i) 0.3 mM IPTG induction at 20ºC, O/N, and (ii) 0.3 mM IPTG induction at 30ºC, during 4h. SDS-PAGE and Western Blot were made in order to select which condition allows the major production of the target protein and the minor production of protein contaminants (Figure 6). To perform this qualitative comparison, the same quantity of bacterial lysate was denatured and deposed on gels, for all samples.

Table 1 – KLC1 constructs whose expression conditions were optimised.

| Protein Code | KLC1 constructs | Limits | Mw (kDa) | Expression vector |
|---|---|---|---|---|
| KLC1_#1 | KLC1-rTEV-His | 206-502 (full TPR domain) | 35,75 | pET22b |
| KLC1_#2 | KLC1-R228D-rTEV-His | | 35,75 | |
| KLC1_#3 | His-Thr-KLC1-GGS-GFP | | 61,92 | pET28 |
| KLC1_#4 | His-Thr-GFP-GGS-KLC1 | | 62,59 | |
| KLC1_#5 | His-Thr-KLC1-GFP | | 61,72 | |

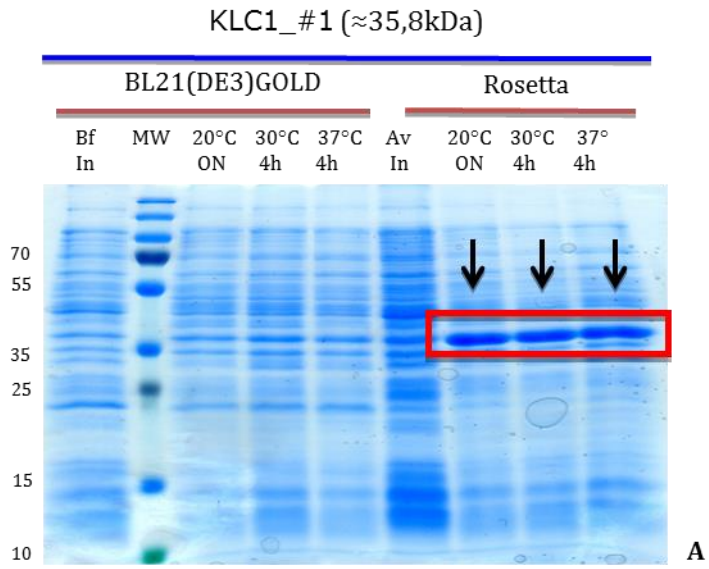
KLC1_#1 (≈35,8kDa)
BL21(DE3)GOLD
Rosetta
Bf In
MW
20°C ON
30°C 4h
37°C 4h
Av In
20°C ON
30°C 4h
37° 4h
70
55
35
25
15
10

A

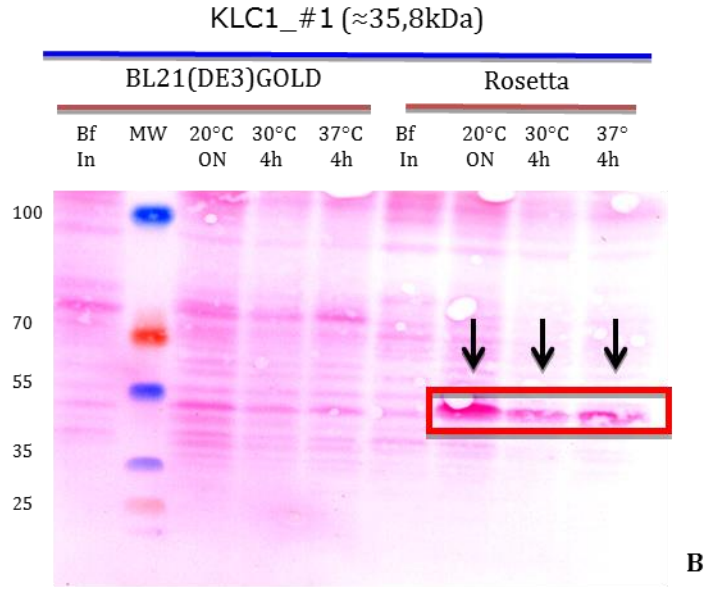
KLC1_#1 (≈35,8kDa)
BL21(DE3)GOLD
Rosetta
Bf In
MW
20°C ON
30°C 4h
37°C 4h
Bf In
20°C ON
30°C 4h
37° 4h
100
70
55
35
25

B

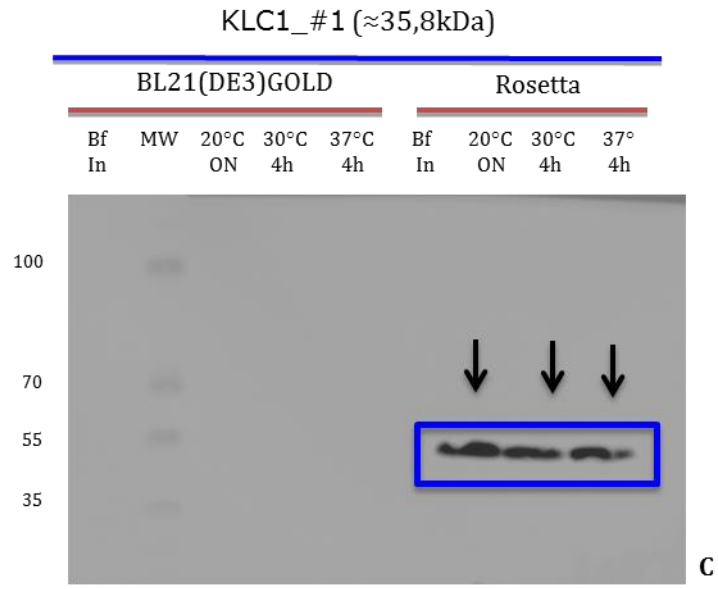


Figure 6 - Expression tests of KLC1_#1. A - SDS-PAGE. B and C - Western Blot performed with the same samples from SDS-PAGE. On B, ponceau red staining shows the protein transferred from the SDS gel to the cellulose membrane. On C, His-tag immuno-detection is shown. On A, B and C it is indicated, by the followed order, the name and molecular weight of the protein, *E. coli* strains used and IPTG induction's time and temperature. On the left of SDS-PAGE and Western Blot images, it is shown the molecular weight of the protein marker used, as well as during all manuscript. Bf In – Before IPTG Induction.

**Solubility and minipurification assays** - After, the selection of favourable protein expression conditions for KLC1 constructs was realized. After, solubility and minipurification tests were realized. Here, it is shown the results of the experiments for KLC1_#1. Same procedures were made for remaining KLC1 constructs (Table 1, results not shown). Using 10 mL of bacterial culture, cell lysis was performed and soluble fraction was separated by centrifugation. Figure 7 shows the results of these experiments and the condition of IPTG induction at 20ºC, O/N, was chosen for minipurification assays. This selection is based on the comparison of soluble/insoluble protein's presence in each condition.

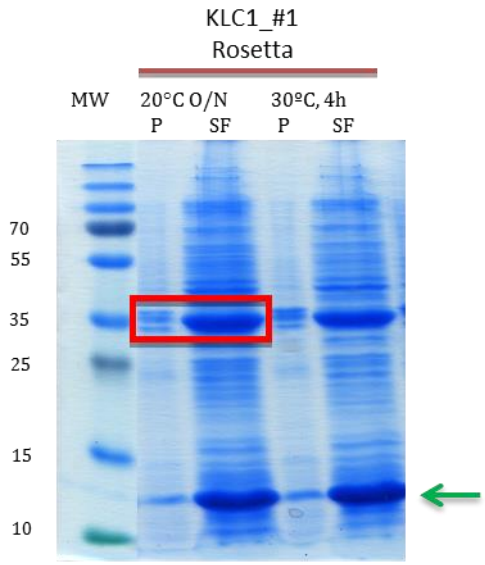


Figure 7 – Bacterial lysis test of the selected conditions for KLC1_#1 protein expression. The red square indicates the condition chosen. The green arrow indicates the presence of lysozyme, used on lysis experiments. P - Pellet (insoluble fraction); SF – soluble.

Figure 7 reveals that both expression conditions have a soluble/insoluble ratio almost similar. Therefore, both conditions are able to be selected for minipurification assays. We chose the first condition to realize minipurification experiments.

The soluble fraction of KLC1_#1 was then incubated with His-tag resins (see Methods), followed by three washes and protein elution was realized. All samples were analysed by SDS-PAGE, in order to visualize qualitatively the purification yield of soluble protein. This strategy was followed for all KLC1 fragments (Table 1). Figure 8 shows the minipurification results for KLC1_#1 fragments. High quantity of target protein was purified during elution step.

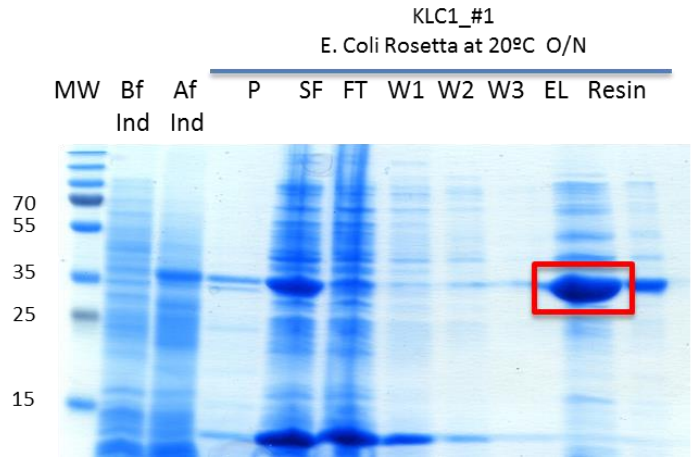


Figure 8 - SDS-PAGE of the minipurification performed for KLC1_#1. As highlighted by the red square, high quantity of target protein was purified during elution. Lysozyme was eliminated during resin's washes. Bf Ind – Before IPTG induction; Af Ind – After IPTG induction; P - pellet (insoluble fraction); SF - soluble fraction; FT – flow through; W – wash; EL – protein elution.

Finally, this experiment confirms that expression conditions selected for KLC1_#1 allow the production of relatively high quantity of soluble protein, capable of being purified by Histidine-tag affinity chromatography. As well, other KLC1 fragments (Table 1) tested gave similar results. Thus, the same expression condition was adopted for all KLC1 constructs which corresponds to *E. coli* Rosetta at 20ºC O/N, with 0.3 mM IPTG induction. We found, by SDS-PAGE, that the migration of KLC1_#1 corresponds to its theoretical molecular weight. Also, there is no target protein quantity eluted from the three washes. During elution, KLC1_#1 was collected with very low presence of contamination.

## Protein Purification Optimization

In order to have a high protein purification yield, all fragments (KLC1 and JIP3_LZII) were purified using an Akta Purifier or Akta Pure System (GE Healthcare). After every purification step, fractions were selected and analysed by SDS-PAGE, aiming the appropriate selection of protein samples to the next purification step or to protein's storage. Hereafter, both chromatogram graph (blue line) and respective SDS-PAGE are shown for each step of the purification process.

**The case of KLC1_#1 -** After lysis and centrifugation of bacteria expressing KLC1_#1, a His-tag affinity chromatography with the protein soluble fraction was performed. Results of this first chromatography step are shown on Figure 9. Here, it is shown higher elimination of protein contaminants during wash step, but also, in the elution step, a huge peak of KLC1_#1. By SDS-PAGE, we confirmed that the elution peak possesses very low protein contamination.

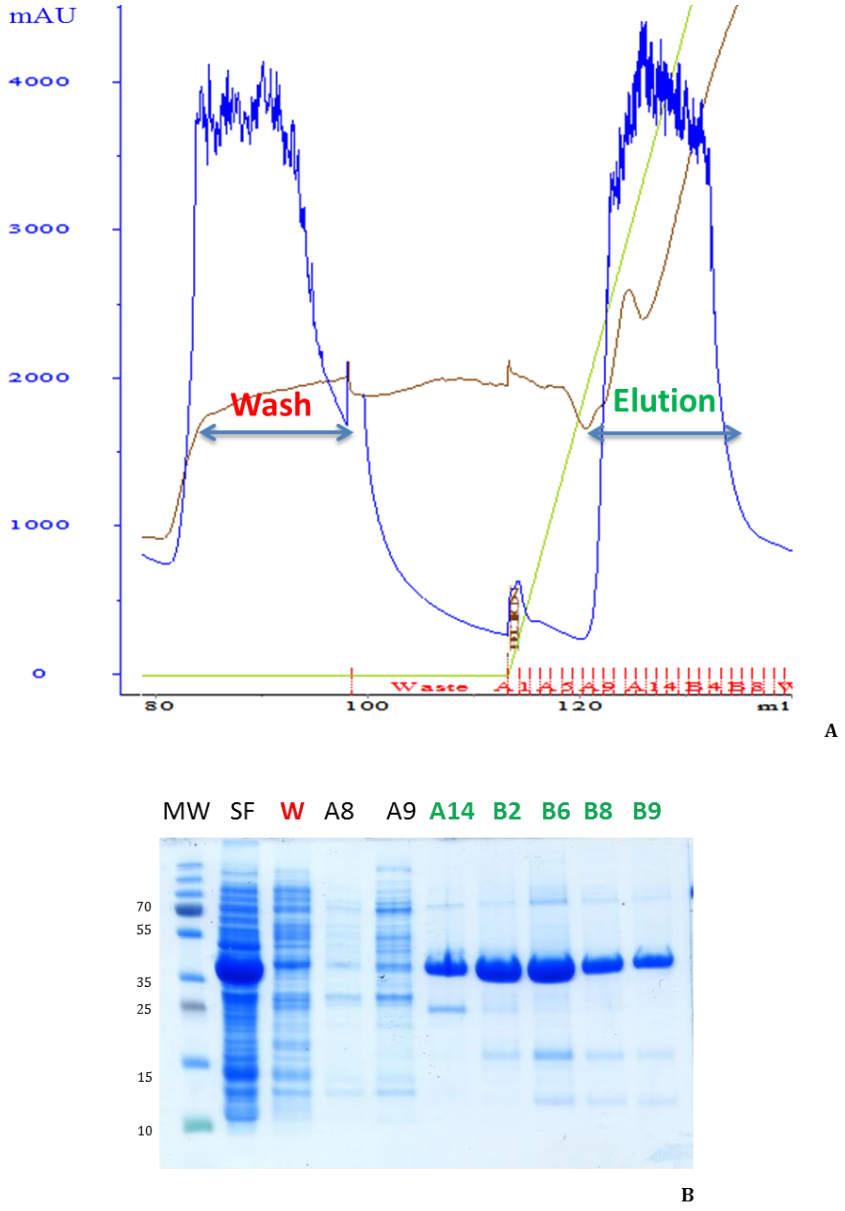


Figure 9 – Purification of KLC1_#1 by His-tag affinity chromatography. A – Elution profile of the His-tag chromatography (blue). It is represented the wash fraction (on red), followed by the elution of the target protein (highlighted on green). B – SDS-PAGE of the His-tag chromatography step. As in A, wash and elution are indicated on red and green, respectively.

Elution fractions were collected (elution peak fractions between A14 and B9 as indicated on figure 9B), concentrated to a final volume of 6 mL, and injected on a HiPrep 16/60 Superdex 75 (GE Healthcare), to perform a gel filtration chromatography as the second purification step.

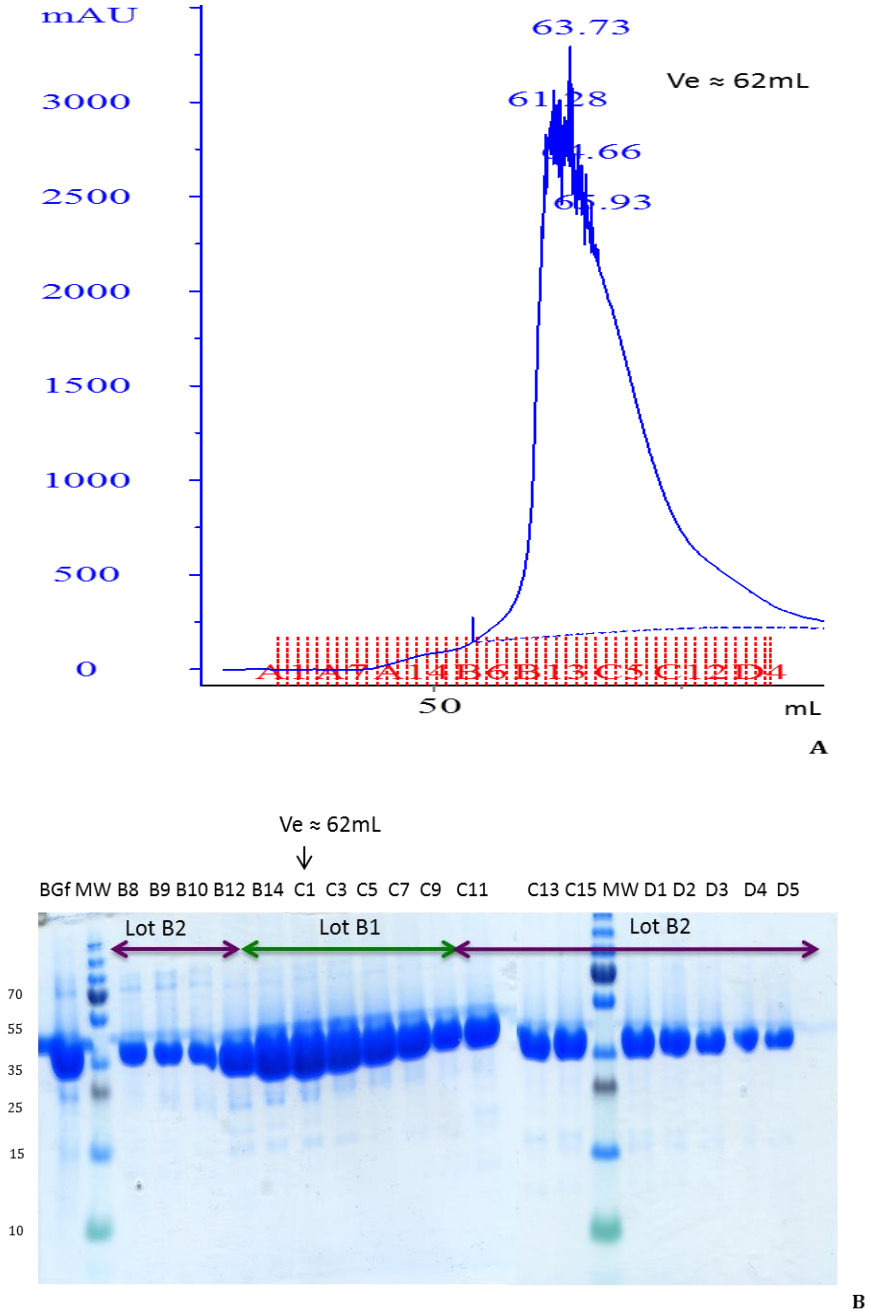


Figure 10 - Purification of KLC1_#1 by gel filtration chromatography. A – Elution profile of the gel filtration chromatography, realized on a HiPrep 16/60 Superdex 75 (GE Healthcare). B – SDS-PAGE of protein samples, testing the gel filtration chromatography step. Here, it is numbered each fraction sample collected. Several fractions were always collected in order to know where the target protein is more concentrated and well purified, with minimum presence of contaminants. It is also indicated two different protein batchs (lots B1 and B2) created to storage JIP3_LZII wild type produced. BGf –protein sample before performing gel filtration. Ve – Elution Volume.

As shown on Figure 10A, the elution volume of KLC1_#1 fragment on the Gel filtration column HiPrep 16/60 Superdex 75 (GE) is around 62 mL. On Figure 10B, two different protein batchs (lots B1 and B2) of KLC1_#1 are indicated, corresponding to low and high protein concentration, respectively. This protein batchs' creation strategy is usually followed by the group, in order to separate and store similar fractions

(qualitatively evaluated by SDS-PAGEs, realized after the gel filtration), but also to have one batch highly concentrated. Finally, two different quantities of protein from each batch are deposed on SDS-PAGE, usually in the order of protein micrograms (ug), aiming a qualitative evaluation of each protein batch, before storage at -80ºC. Thus, we made a SDS-PAGE (Figure 11) that reveals the highly purity of KLC1_#1 with no presence of protein contaminants.

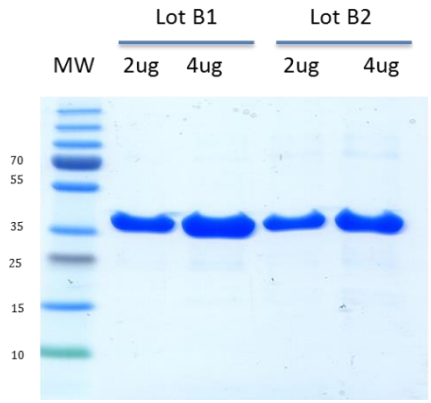


Figure 11 – SDS-PAGE of KLC1_#1 batchs.

**KLC1 purification: an overview -** In order to have a high yield of purification, two different chromatography steps were performed for all KLC1 fragments. In each case, firstly, His-tag affinity chromatography was realized, aiming the elimination of the major part of the contaminants from soluble fraction of bacterial lysate. In consequence, a gel filtration was performed, polishing KLC1 fractions obtained before, aiming a high yield of protein purity and conformational homogeneity. Protocol was similar for all KLC1 fragments and the yield of protein production (mg of protein/ liter of expression culture) is shown on Table 2, as well as their storage buffer. We obtained two different ranges of protein yield. The presence of GFP probably stabilizes protein fragments produced, allowing high quantity of these proteins produced (KLC1_#3, KLC1_#5). On the other hand KLC1_#1, KLC1_#2 and KLC1_#4 are probably less stable.

After protein purification, all KLC1 fragments were stored in 1 mL fractions, frozen in liquid nitrogen and stored at -80ºC. Annexe 4 shows all the buffers used during the purification steps, which were also optimised.

Table 2 - KLC1 fragment yield after purification.

| KLC1 mutant code number | Protein yield (mg /L) | Storage Buffer |
|---|---|---|
| KLC1_#1 | 74 | 50 mM HEPES pH 8.0, 200 mM NaCl |
| KLC1_#2 | 70 | |
| KLC1_#3 | 160 | |
| KLC1_#4 | 80 | |
| KLC1_#5 | 152 | |

## JIP3_LZII mutants

### Expression Conditions Optimisation

**Protein expression tests** - Expression tests were carried out for JIP3_LZII_#1, wild type fragment (Table 3). We assumed an equivalent expression yield for all JIP3_LZII wild type and mutants, independently on the mutation. The successful of the strategy was proved by equivalent purification yield between the considered JIP3_LZII wild type and mutants (shown on JIP3 purification results). All JIP3_LZII constructs have human origin, consisting on JIP3 residues 416-486 and share a molecular weight around 35,60 kDa. They are cloned in a pGST expression vector and thus are produced with a GST-tag and rTEV cleavage site.

Table 3 – List of JIP3_LZII constructs.

| JIP3_LZII code | Mutation position on coiled-coil | Mutation |
|---|---|---|
| JIP3_LZII_#1 | - | Wild type |
| JIP3_LZII_#2 | Second heptad | Protein mutants performed by Alanine Scanning on the LZII heptads. #8 is the charge reversion mutation. |
| JIP3_LZII_#3 | Second heptad | |
| JIP3_LZII_#4 | Third heptad | |
| JIP3_LZII_#5 | Third heptad | |
| JIP3_LZII_#6 | Fourth heptad | |
| JIP3_LZII_#7 | Fourth heptad | |
| JIP3_LZII_#8 | Fourth heptad | |
| JIP3_LZII_#9 | Fifth heptad | |
| JIP3_LZII_#10 | Third heptad | |
| JIP3_LZII_#11 | Fourth heptad | |

As well as for KLC1 expression optimisation, the same procedures were performed for JIP3_LZII_#1. Here, it is also tested the presence of 1% ethanol in the expression conditions, aiming the induction of stress conditions and bacterial response on protein expression. In Figure 12A, the results of JIP3_LZII_#1 (Table 3) expression tests are shown.

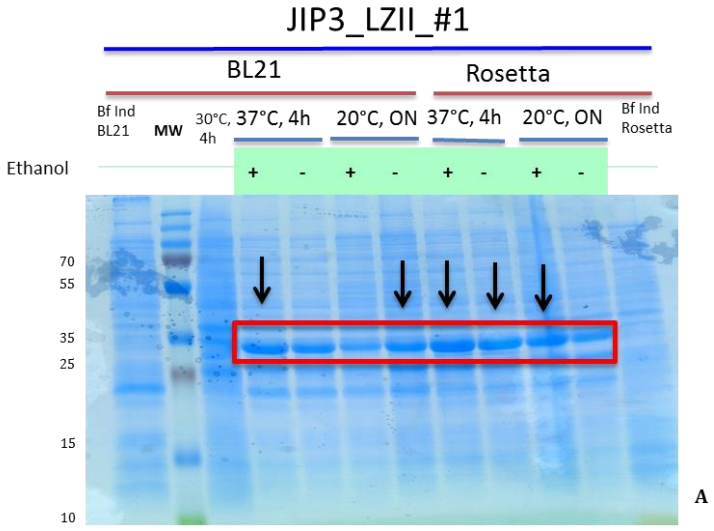


A

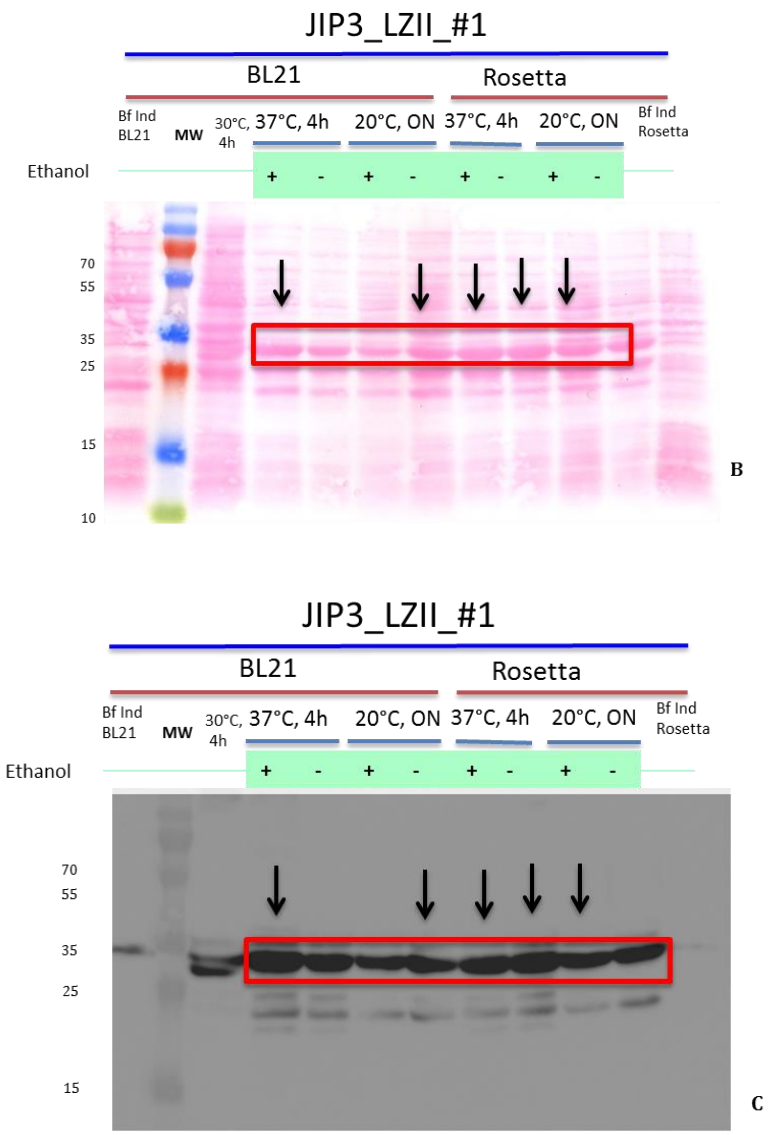


Figure 12 - Expression tests of JIP3_LZII_#1. A - SDS-PAGE performed in 9 different conditions. B and C - Western Blot performed with the same samples from SDS-PAGE (A). On B, ponceau red staining shows the protein transferred from the SDS gel to the cellulose membrane. On C, GST-tag immuno-detection is shown, demonstrating the presence of the target protein.

At this point, several conditions were found as favourable to realize solubility and minipurification tests. JIP3_LZII_#1 possesses good expression yields in almost of every conditions tested. On Figure 12C, it is possible to detect and predict that there are also GST-protein contaminants which are present in these expression conditions. The followed expression conditions (Table 4) were selected for the next step, taking in consideration the major production of the target protein as well as the minor production of protein-tagged contaminants (Figure 12).

Table 4 – JIP3_LZII_#1 expression conditions selected for solubility and minipurification tests.

| ***E. coli* strain** | **Indution time** | **Temperature (ºC)** | **1% Ethanol** |
|---|---|---|---|
| BL21(DE3)GOLD | 4h | 37 | + |
| BL21(DE3)GOLD | O/N | 20 | - |
| Rosetta | 4h | 37 | + |
| Rosetta | 4h | 37 | - |
| Rosetta | O/N | 20 | + |

**Solubility and minipurification assays** - Based on this selection, solubility and minipurification tests were realized for JIP3_LZII_#1. Figure 13 and 14 show the results of these experiments. For each condition, 10 mL of bacterial culture was lysed and soluble fractions were separated by centrifugation. The condition using *E. coli* BL21(DE3)GOLD, with 0.3 mM IPTG induction and temperature of 20ºC, O/N, without ethanol was the chosen one to be analysed by minipurification assays. This selection is based on the comparison of the soluble/insoluble ratio protein in each condition, after bacterial lysis. The goal is to select the expression condition with the higher ratio value, in order to obtain soluble protein target on the best quantity as possible. As it is demonstrated by SDS-PAGE of these experiments (Figure 13), the chosen condition (highlighted on red), possesses a higher quantity of target protein on the soluble fraction.

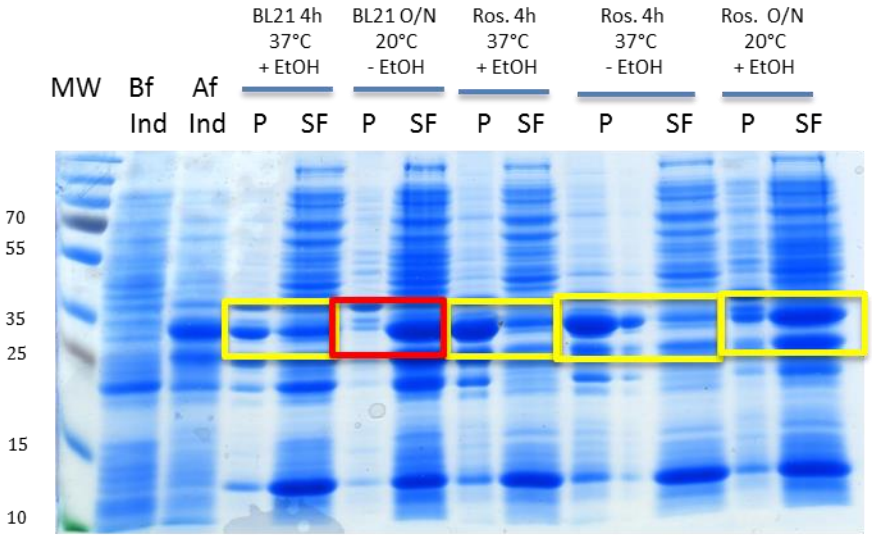


Figure 13 - Lysis tests of the selected conditions for JIP3_LZII_#1 protein expression. The expression condition of BL21(DE3)GOLD, 20ºC O/N, without ethanol, was chosen (highlighted on red). In comparison with the remaining conditions (highlighted on yellow), the chosen condition shows higher presence of soluble protein, EtOH – Ethanol; Bf Ind – Before Induction; Af Ind – After Induction. P - Pellet (insoluble fraction); SF - soluble fraction.

Thus, the soluble fraction of JIP3_LZII_#1 selected was incubated with GST-tag resins, then washed three times and protein elution was consequently realized. All samples were analysed by SDS-PAGE, in order to visualize, qualitatively, the yield purification of JIP3_LZII_#1 (Figure 14).

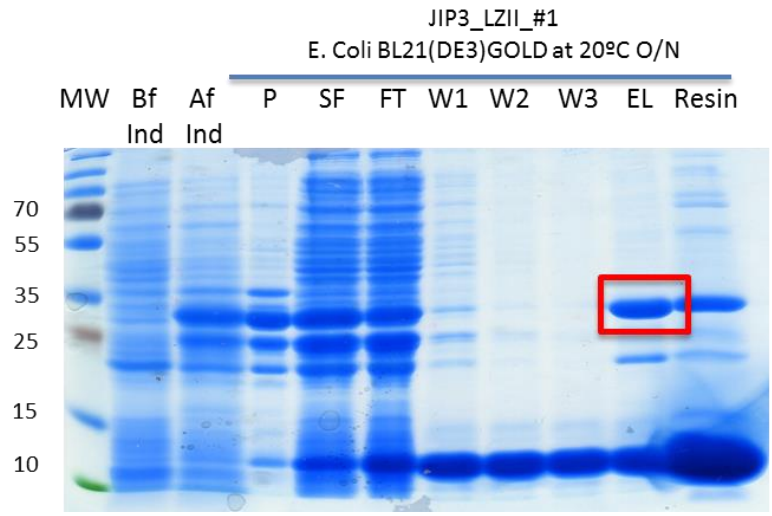


Figure 14 - SDS-PAGE of the minipurification performed for JIP3_LZII_#1. As highlighted by the red square, high quantity of target protein was purified during elution. Lysozyme was eliminated during resin's washes. Bf Ind – Before IPTG induction; Af Ind – After IPTG induction; P - pellet (insoluble fraction); SF - soluble fraction; FT – flow through; W – wash; EL – protein elution.

Finally, we confirmed that expression conditions selected for JIP3_LZII_#1 produce high quantity of soluble protein, capable of being purified by GST-tag affinity chromatography. We used the expression condition found to all JIP3_LZII mutants with similar results as for JIP3_LZII wild type. We found, by SDS-PAGE, that the migration of JIP3 fragment corresponds to its theoretical molecular weight. Also, there is no target protein eluted from the three washes. However, a significant protein contaminant was eluted with JIP3_LZII_#1, during the elution step.

## Protein Purification Optimization

**The case of JIP3_LZII_#1 (wild type) -** The description presented is similar to all JIP3_LZII mutants and, here, I show the results for JIP3_LZII_#1.

The first purification step is an affinity chromatography using GST-trap. This step allowed to collect the protein of interest, but also a GST-protein contaminants of

lower molecular weight, as shown on Figure 15. Collected fractions contain high quantity of the target protein; however, an important GST-contaminant around of 25 kDa is present in the elution. As confirmed on its expression tests, by western blot, this protein contaminant possesses GST-tag, which represents a difficulty to highly purify the target protein. However, high quantity of JIP3_LZII_#1, GST-tagged, was collected.

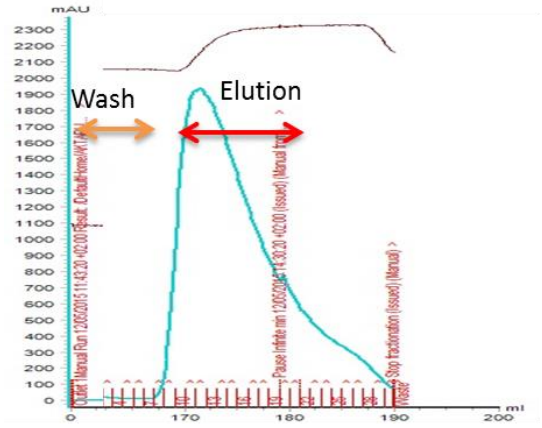


Figure 15 – First GST-tag affinity chromatography performed for JIP3_LZII wild type. A – Elution profile detected by Abs 280nm (blue line). B – SDS-PAGE showing the results of this chromatography step. It is highlighted on red the samples collected and tested from JIP3_LZII_#1 elution.

Thus, I collected desirable protein fractions, mixed them and quantified by Bradford methods. I added rTEV protease with a ratio of 1:20, in order to cleave and eliminate the GST-tag from JIP3_LZII_#1. Therefore, protein sample and protease were incubated at 10°C, O/N. The protease products are illustrated on Figure 16.

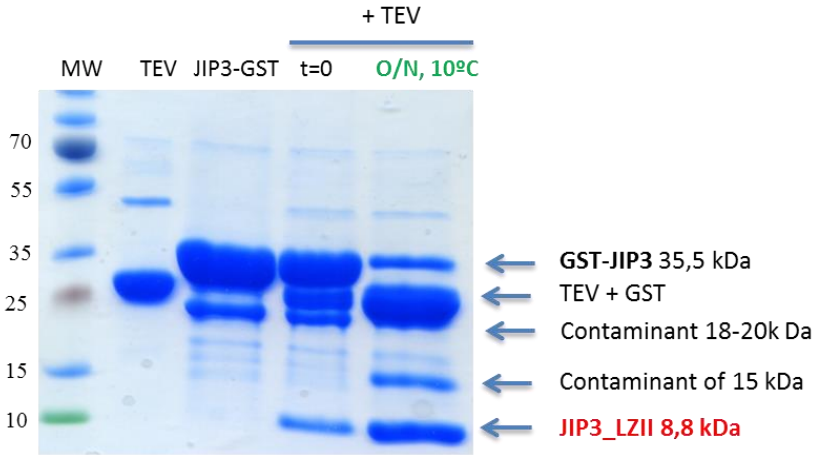


Figure 16 - SDS-PAGE illustrating the results of rTEV protease activity on GST-JIP3_LZII_#1. It is shown rTEV and JIP3_LZII_#1 samples separated, as well as the proteolysis at t=0 and O/N. After cleavage O/N by rTEV, there were several protein products, identified on the figure. The target protein (JIP3_LZII) is highlighted on red.

In order to eliminate rTEV, which is His-tagged, I performed a second affinity chromatography using 5mL His-Trap column. Interestingly, this step of purification should also remove His-protein contaminants. During the purification optimisation process, we found that it is essential to perform this chromatography, aiming the total elimination of the protease contamination products. Then, in order to eliminate GST-tagged contaminants (GST, contaminant GST-tagged fragments and JIP3 with GST-tag not cleaved), I realized the second GST-trap chromatography (third affinity chromatography step). In both His-trap and GST-trap steps, the flow through was kept since JIP3_LZII_#1 (already cleaved) is retained neither by His- nor by GST- columns. These steps highly reduce the quantity of contaminants which were with the protein target, as shown on Figure 17 and 18.

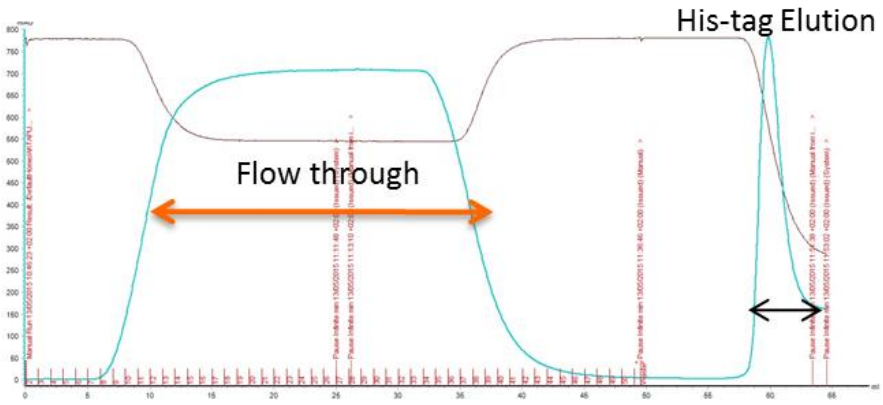


**A**

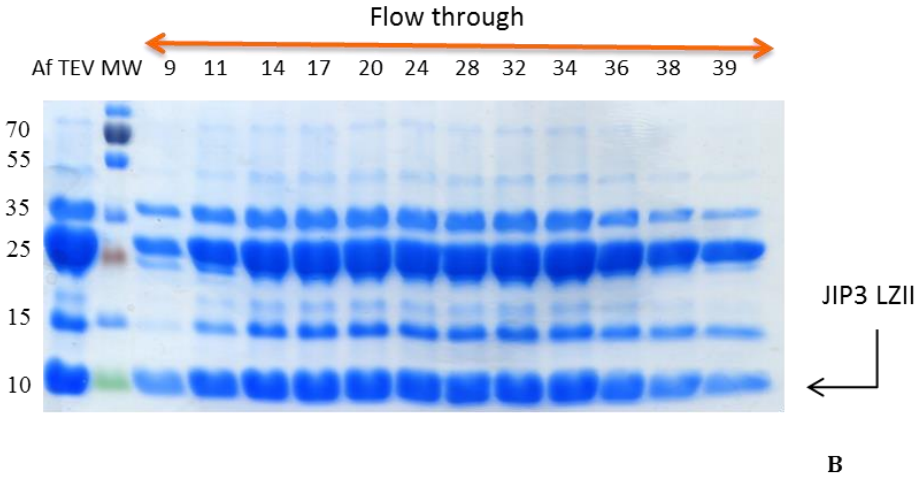


Figure 17 - Elimination of His-tag contaminants. His-tag chromatography performed in order to eliminate rTEV and all possible His-tag products from the protein sample. On A, protein elution profile (blue line) of the chromatogram, indicating the flow through fractions recovered. On B, analysis of protein samples collected on flow through, by SDS-PAGE. Af TEV – protein sample after rTEV cleavage

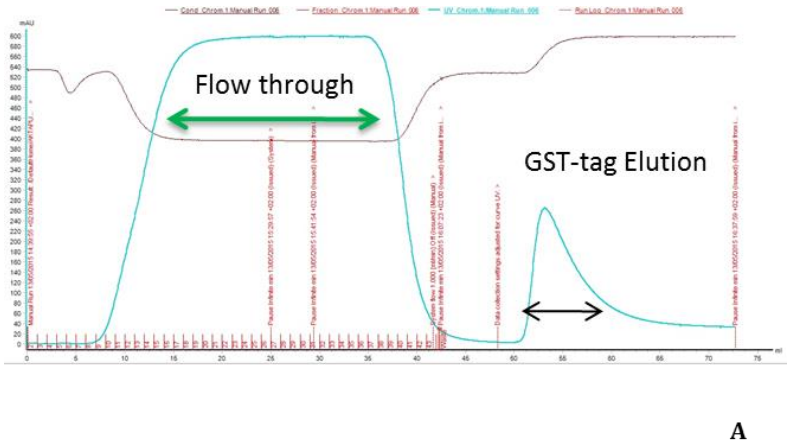


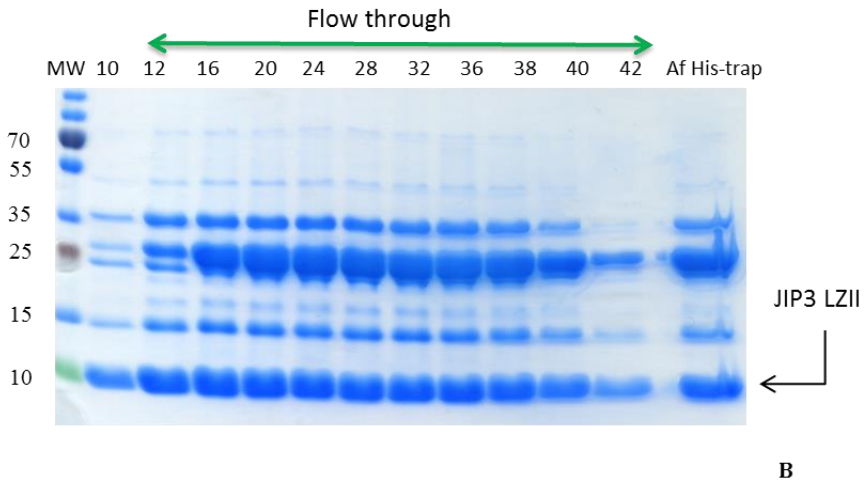


Figure 18 – Elimination of GST-tag contaminants. GST-tag chromatography performed aiming the elimination of all GST contaminants. On A, protein elution profile (blue line) of the chromatogram, indicating the flow through fractions recovered. On B, analysis of protein samples collected on flow through, by SDS-PAGE. Af His-trap – protein sample collected from the His-trap flow through.

After recovering the selected flow through protein fractions (on His- and GST-tag affinity chromatographies), I concentrated JIP3_LZII_#1 fractions into 6 mL (as described), allowing its injection on a gel filtration column HiPrep 16/60 Superdex 75 (GE Healthcare). During this final chromatography step, there were two different elution volumes where contaminants were eliminated, and finally JIP3_LZII_#1 was eluted, starting at the column elution volume around of 100 mL, until the final of the column volume, corresponding, theoretically, to a globular protein of the molecular weight around 8-10 kDa. Size exclusion chromatography results are shown on Figure 19.

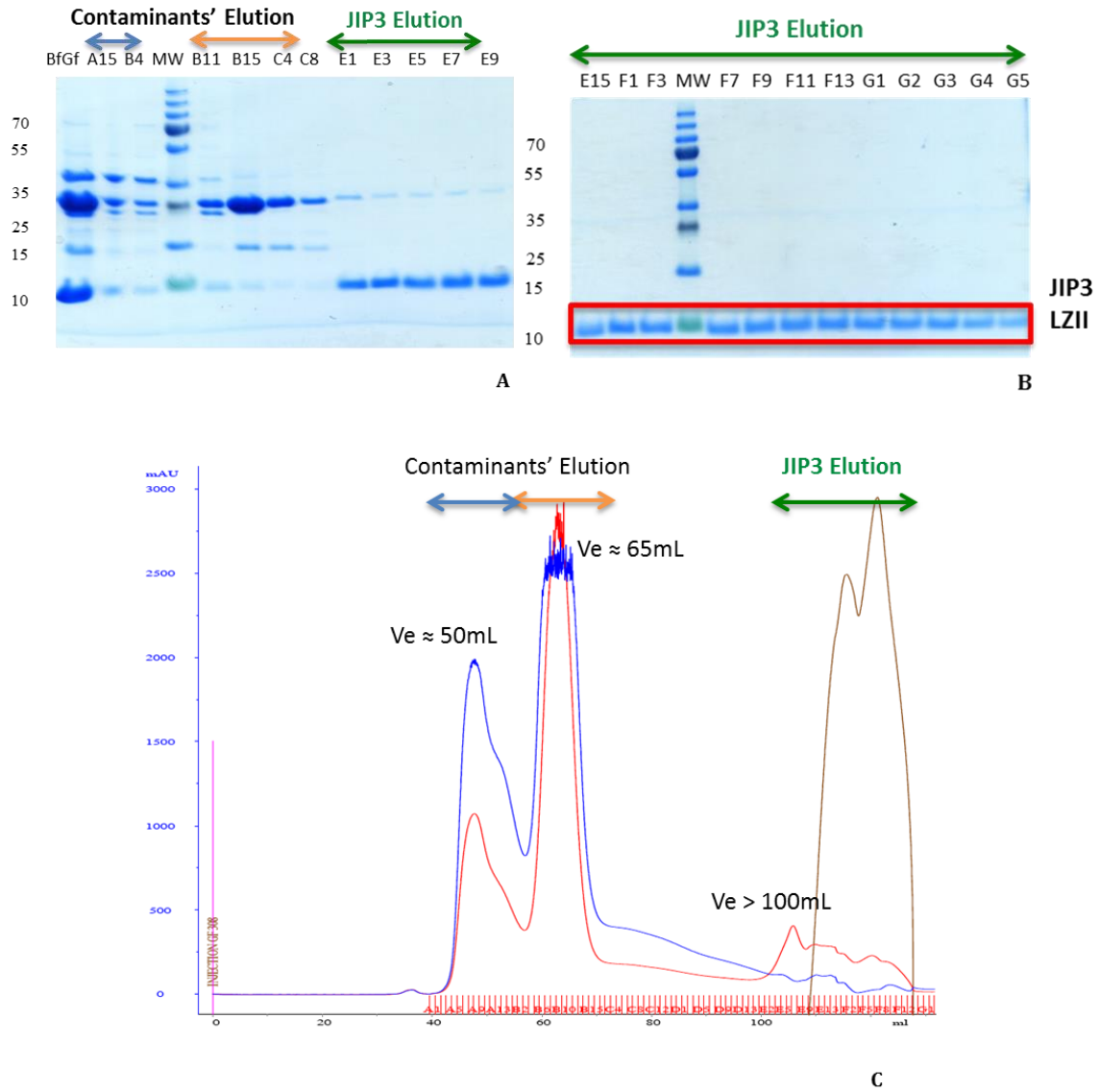


Figure 19 – Size exclusion chromatography results of JIP3_LZII_#1. On A, B and C, it is highlighted by blue and orange arrows, two protein elution peaks, corresponding to different contaminant elution volumes (around 50 and 65 mL). On green, it is highlighted JIP3_LZII elution, from the volume of 100 mL until the final of the size exclusion column volume. A and B – SDS-PAGE showing the different elution moments from the size exclusion elution step. On red square, JIP3_LZII_#1 is highlighted. C – Size exclusion chromatogram. Protein elution was better followed by Abs254 (red line).

Finally, I collected and tested protein samples from the third elution moment (highlighted by a red square on figure 19B). I measured JIP3_LZII_#1 concentration by Abs 280 nm and concentrated it for storage. I also performed a gel batch (Figure 20), aiming a qualitative analysis of the protein purity, before storage at -80ºC. I deposed two different JIP3_LZII_#1 quantities and compared also with same BSA quantities. On the figure, similar protein band intensities were detected, between JIP3_LZII_#1 and BSA, in the respective quantities (1 and 2 ug). This evidence allowed a qualitative confirmation that concentration measures of this protein by Abs 280 nm highly approaches its real concentration value.

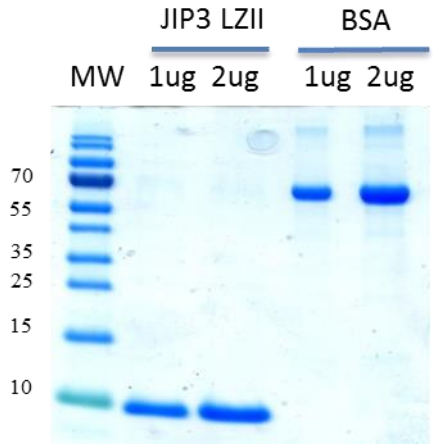


Figure 20 - SDS-PAGE batch of JIP3-LZII purified.

**JIP3_LZII purification: an overview -** After several trials and different protocols and strategies tested, JIP3_LZII_#1 was purified successfully, with very low contamination. Therefore, the same protocol was used for all JIP3_LZII mutants. Five different protein purification steps were required, as explained above to the case of JIP3_LZII_#1, also summarized on Figure 21. On the scheme, each purification step is illustrated, as well as the loss of protein quantity by the represented arrows, between each purification step realized.

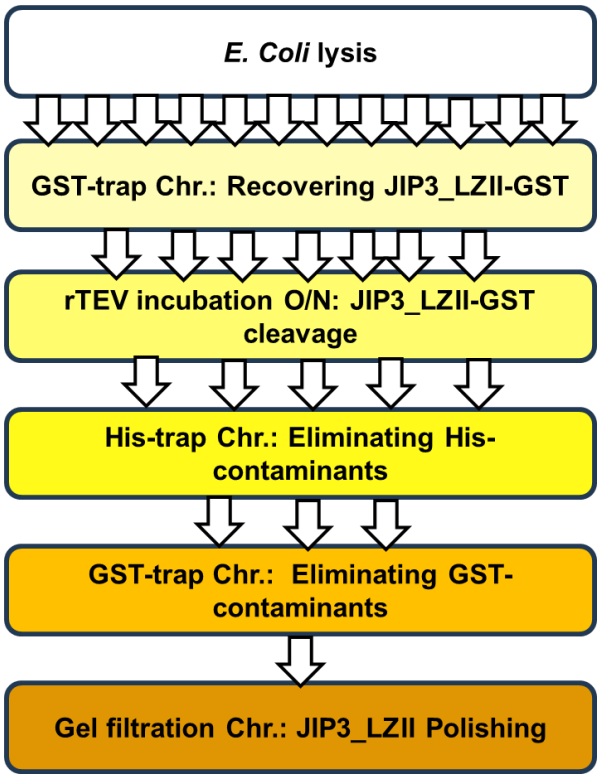


Figure 21 - Resume of JIP3_LZII purification strategy optimised. Chr. - Chromatography

On Table 5, I present the list of JIP3_LZII mutants that we purified and their yield (mg of protein/L of bacterial culture).

Table 5 – Purification yield of JIP3_LZII mutants. Storage buffer is also indicated.

| JIP3_LZII mutants | Purification yield (mg of target protein/L of bacterial culture) | Storage Buffer |
|---|---|---|
| JIP3_LZII_#1 | 0,90 | 50mM Tris pH 8.0, 150 mM NaCl, 0,05% Tween |
| JIP3_LZII_#2 | 1,18 | |
| JIP3_LZII_#3 | 0,94 | |
| JIP3_LZII_#4 | 0,50 | |
| JIP3_LZII_#5 | 2,00 | |
| JIP3_LZII_#6 | 0,70 | |
| JIP3_LZII_#7 | 0,28 | |
| JIP3_LZII_#8 | 1,17 | |
| JIP3_LZII_#9 | 1,05 | |
| JIP3_LZII_#10 | 0,92 | |
| JIP3_LZII_#11 | 1,03 | |

All the strategy was optimised, taking in consideration the importance of having highly purified protein, with no contamination. During all JIP3s' protein purification, a high level of purity was achieved; however, their yield (mg of purified protein/ liter of bacterial culture) is weak, also due to a high number of purification steps performed. Despite of low JIP3_LZII yield, important quantities of all protein mutants were produced and used successfully, as described on the next topics.

Interestingly, we found that the yield of JIP3_LZII_#7 is lower, comparing with other JIP3_LZII fragments. Generally, the value for JIP3_LZII fragments is around 1 mg/L. However, JIP3_LZII_#7 shows a purification yield of 0.28 mg/L.

All buffers used during these JIP3_LZIIs' purification are indicated on Annexe 4.

## Protein Production already optimised

During the course of the project, I performed the production and purification of other KLC1 fragments, as well as JIP4 fragments, whose expression and purification protocols were already optimised on the laboratory. Their expression and purification protocols are not mentioned on this report because they were not relevant for the project in study. These proteins were used for KLC1:JIP3/4 interaction experiments (MST, SAXS). Also, I produced rTEV protease to handle during JIP3_LZIIs' purification protocol.

On Table 6 these proteins are presented, as well as their storage buffers.

Table 6 – rTEV, KLC1 and JIP4 fragments produced during the project.

| Protein Code | Protein fragments | Storage Buffer |
|---|---|---|
| rTEV | His-rTEV | 50 mM Tris pH 8.0 ; 200 mM NaCl ; 25% glycerol, EDTA DTT 1mM pH 8.0 and DTT 1mM pH 8.0 |
| KLC1_#0 | His-KLC1-TPR6 | 50mM HEPES pH8; 200mM NaCl |
| JIP4_LZII_#1 | His-JIP4-WW | 50 mM HEPES pH7, 50 mM NaCl, 5 mM MgCl2, 0,05% Tween20, 1 mM DTT |

## *As a short revision…*

Table 7 shows all protein fragments for which production and purification have been described previously. Altogether, these proteins have been used for protein characterization and protein-protein interaction experiments.

Table 7 - Overview of all protein fragments produced during this project.

| **Protein fragments handled during the project** | **Protein Code** |
|---|---|
| **KLC1s** | KLC1_#0<br>KLC1_#1<br>KLC1_#2<br>KLC1_#3<br>KLC1_#4<br>KLC1_#5 |
| **JIP3_LZIIs** | JIP3_LZII_#1<br>JIP3_LZII_#2<br>JIP3_LZII_#3<br>JIP3_LZII_#4<br>JIP3_LZII_#5<br>JIP3_LZII_#6<br>JIP3_LZII_#7<br>JIP3_LZII_#8<br>JIP3_LZII_#9<br>JIP3_LZII_#10<br>JIP3_LZII_#11 |
| **JIP4_LZII** | JIP4_LZII_#1 |
| **His-rTEV** | rTEV |

# Protein Characterization

We aimed to structurally characterize all the fragments produced in order to have information about structural integrity, stoichiometry of the protein, but also to find better buffer conditions to handle with them.

## Characterization of the Structural Integrity of KLC1

**Limited proteolysis experiments of KLC1 fragments: overview -** In the course of this project, I performed limited proteolysis for KLC1_#1, KLC1_#3 and KLC_#4. KLC_#5 was not yet tested. For the protein mutant KLC1_#2, it was considered that its point mutation would not affect its folding. KLC1 proteins tested had similar results.

We aimed, performing this methodology, to have evidences of the correct protein fragments' folding. Here, it is described the results for KLC1_#1, which was incubated, separately, with 9 different proteases (with different cleavage sites; see Materials and Methods). In these experiments, it is shown by SDS-PAGE (Figure 22) that KLC1_#1 was resistant to proteolysis, maintaining its molecular weight. Thus, KLC1_#1 is not sensitive to these 9 proteases, suggesting that it is well folded. Interestingly, KLC1_#1 and KLC1s tested possess a proteolysis cleavage site to eliminate His-tag. Theoretically, rTEV should cleave KLC1_#1 and thrombin should cleave KLC1_#3 and KLC1_#4. For these fragments, it was also tested O/N incubation (results not shown) and we found different proteolysis yields in these cases. Therefore, we assume that, for these KLC1 fragments, proteolysis cleavage sites conceived for His-tag elimination are not completely accessible on the surface of the proteins. During the incubation time of 30 minutes, no protease activity was reported. Also, with O/N incubation, different results were obtained.

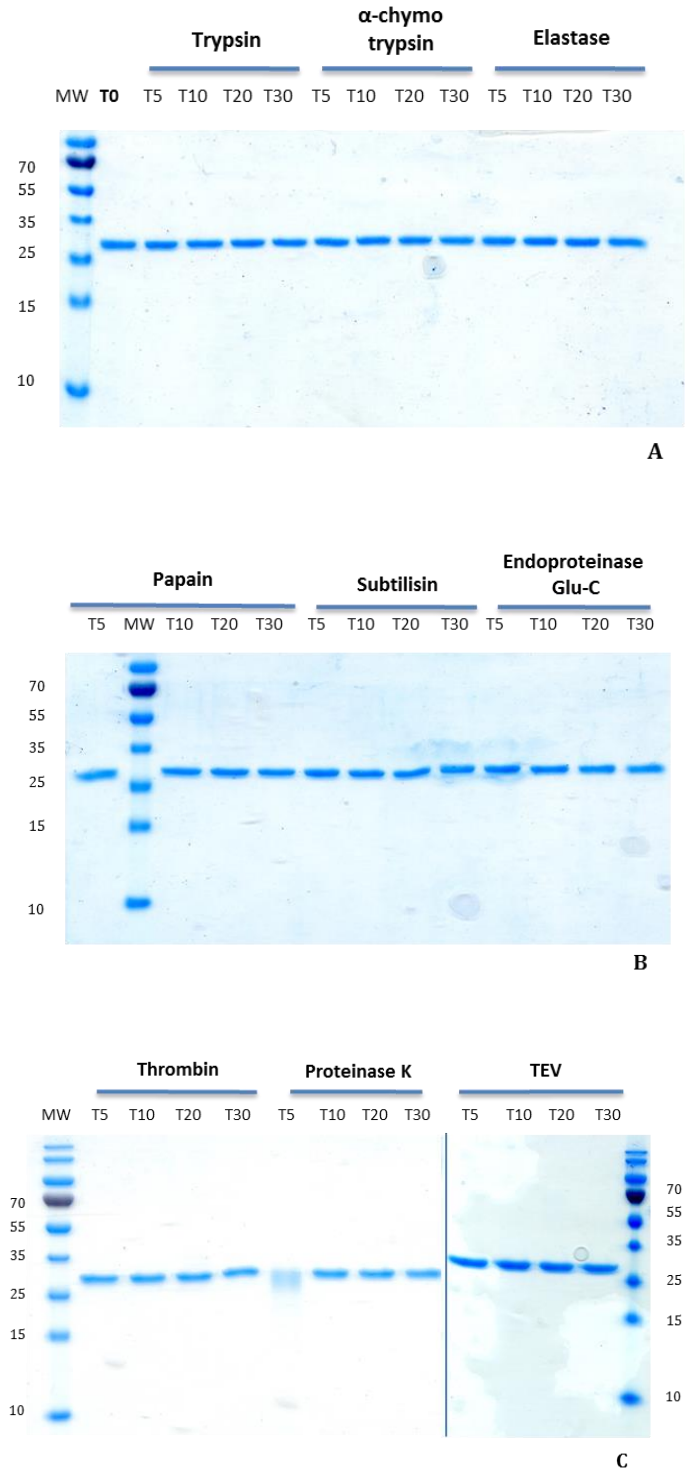


Figure 22 - Limited proteolysis experiments performed for KLC1_#1. In A, B and C, SDS-PAGEs are shown and indicated for each sample the time of exposure (T/min) of KLC1_#1 to each protease.

**Thermal Shift Assays of KLC1 fragments -** I performed Thermal Shift Assay on KLC1_#1 and KLC1_#3 fragments, aiming to have information about the melting temperature and thus, indirectly, on folding stability of these fragments on different buffer conditions. Also, the main purpose is to find the better buffer conditions where proteins will be stable, allowing to perform biophysical experiments. Figure 23 shows the melting temperatures calculated (mean from triplicate measures) for proteins in study. Numbered buffers used as TSA conditions tested and detailed results are described in Annexe 5.

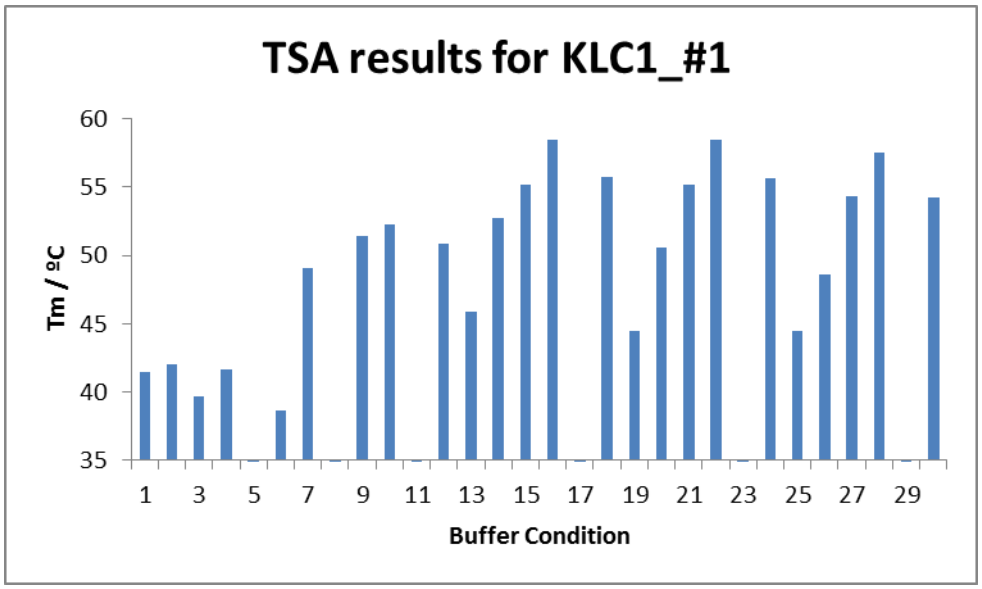


A

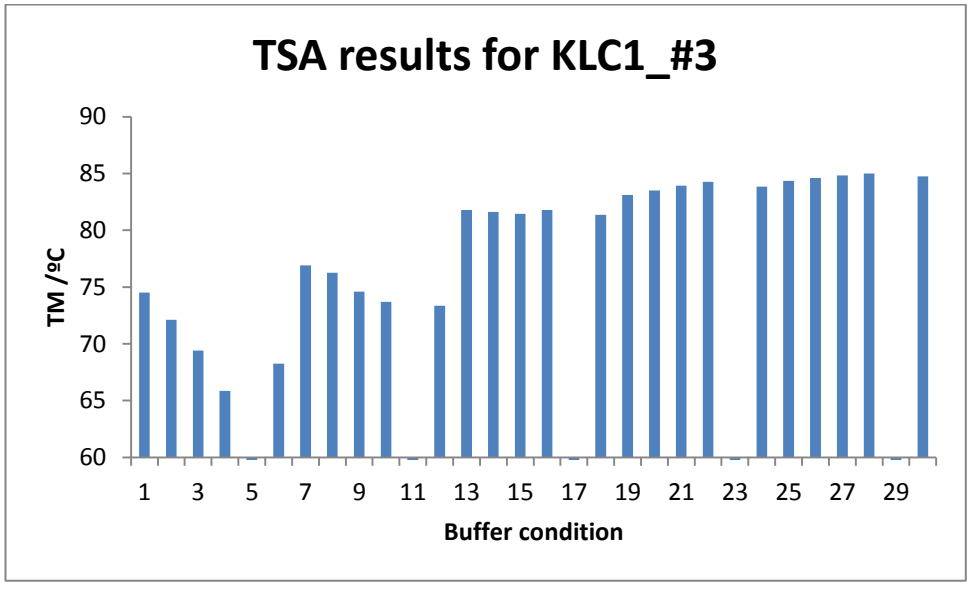


B

Figure 23 - TSA results for KLC1_#1 (A) and KLC1_#3 (B).

According to the results (best conditions shown below on Table 8), KLC1_#1 has melting temperatures in the range of 55-59°C, showing very high stability in the presence of Hepes pH 7.0 or Tris pH 8.0 and in the range NaCl concentration of 0.2-0.5 M, or 0.2 M KCl.

Table 8 - Buffer conditions tested for KLC1_#1, by TSA, with higher melting temperatures. These values were calculated taking in consideration a triplicate measurement of each sample. It is shown their average and standard deviation. s (Tm) – standard deviation of melting temperatures registered.

| Buffer /50 mM | NaCl /M | KCl /M | Tm /°C | s (Tm) /ºC |
|---|---|---|---|---|
| Hepes pH 7.0 | 0,2 | 0 | 55,13 | 0,17 |
| | 0,5 | | 58,44 | 0,09 |
| | 0 | 0,2 | 55,71 | 0,09 |
| Tris pH 8.0 | 0,2 | 0 | 55,16 | 0,09 |
| | 0,5 | | 58,49 | 0,09 |
| | 0 | 0,2 | 55,61 | 0,00 |
| Glycine pH 9.0 | 0,5 | 0 | 57,52 | 0,09 |

Due to the results achieved, KLC1 storage buffer (50 mM Hepes pH 8.0; 200mM NaCl) was maintained after Thermal Shift Assay experiments. These buffer conditions were already satisfying, keeping the folding stability of the protein.

Concerning KLC1 constructs fused to GFP (KLC1_#3 tested), it was established melting temperatures in the range of 80ºC. We expected to have two melting temperatures, correspondent to KLC1 and GFP parts of the protein-fusion. However, it was found that the fusion of GFP fragment to KLC1 increases the melting temperature of the overall protein. Probably GFP stabilizes KLC1, through direct interaction. Thus, it is not possible to obtain conclusive results in terms of buffer conditions and the correct folding of the KLC1 part of the protein-fusion. Thus, it was assumed that same conditions as for KLC1_#1 would be also favourable.

TSA experiments were also realized for JIP3_LZII fragments, however without significant results. Considerable quantity of Tween 20 is present on the storage buffer of these proteins. This chemical detergent highly interferes in the results of TSA, probably interacting directly with Sypro Orange. Both have hydrophobic characteristics. Therefore, Thermal Shift assays were not adopted for JIP3_LZII.

**SEC-MALS experiments of KLC1 fragments -** KLC1_#1, KLC_#3 and KLC_#4 fragments, similarly with limited proteolysis, were tested in order to characterize the molecular mass of the proteins in solution, and thus their oligomeric state. SEC-MALS analysis allowed the confirmation of the homogeneity and the monomeric state of KLC1 fragments tested. The theoretical molecular weight of KLC1 fragments is similar to measured values by this technique. Below, on the Table 9, results are shown and, on Figure 24, the graphical analysis for protein KLC1_#1 (remaining graphical results not shown). Of note, KLC1_#3 and KLC1_#4 are fused with GFP (26.8 kDa).

Table 9 - Analysis data from SEC-MALS experiments performed for KLC1 fragments. For all cases, there was only a single KLC1 elution peak. Values between parenthesis are correspondent to the maximum values of light diffusion.

| | KLC1_#1 | KLC_#3 | KLC_#4 |
|---|---|---|---|
| Theoretical Molecular Weight | 35.6 kDa | 66.3 kDa | 62.4 kDa |
| Peak limits (mL) | 15.014 – 16.301 (15.527) | 13.282 – 15.104 (14.023) | 13.492 – 15.139 (14.121) |
| dn/dc (mL/g) | 0.183 | 0.183 | 0.183 |
| Mean of Molecular Weight (kDa) | 39.79 ± 0.17 (40.04) | 65.07 ± 0.16 (66.29) | 62.09 ± 0.15 (6.244) |
| Hydrodynamic radius | 1.9 ± 0.2 (1.9) | 2.8 ± 0.2 (3.0) | 2.4 ± 0.2 (2.5) |

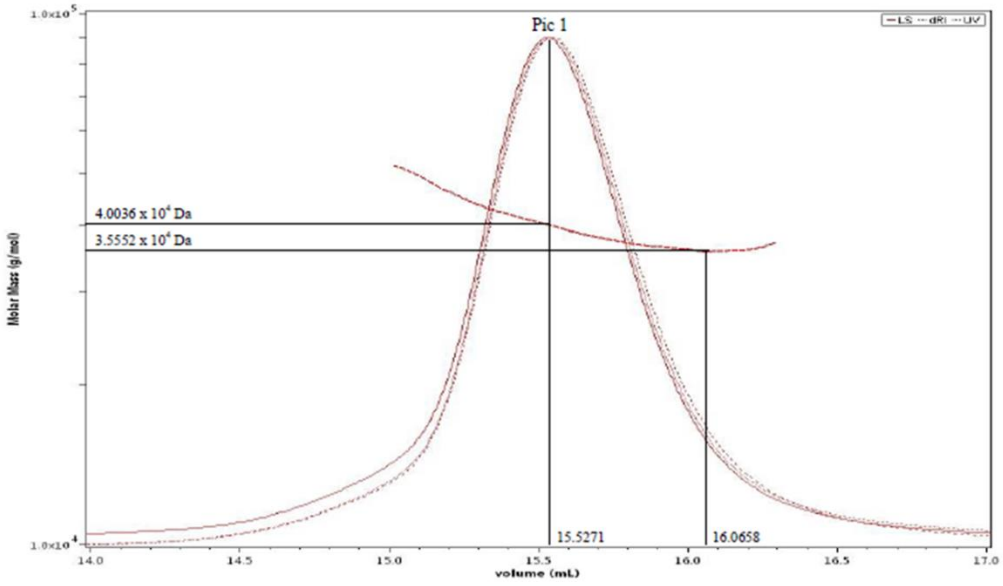


Figure 24 - Zoom of the elution chromatogram of KLC1_#1 in a Superdex 200 10/300 GL Increase. Red line: light scattering; Dashed line: dRI signal; pointed line: UV 280 nm signal.

There were two KLC1 fragments which were not tested by SEC-MALS. For the protein KLC1_#2, it was predicted by its 3D structure (already known, see Introduction) that the point mutation would not affect its protein folding. This residue is in the tight turn that connects helix 1 to helix 2 of the TPR1 motif of the TPR domain. The side chain of the arginine is exposed toward the solvent making no interaction with other residues on the TPR domain.

**Protein Crystallization assays of KLC1_#1 -** Protein KLC1_#1, produced and characterized in the course of this project, was used also in other laboratory's project. The 3D structure was already published, and here, the goal was to obtain protein crystals with a X-ray resolution less than 3.0 Å, aiming to perform peptide soakings with other partner (for other project of the lab, not developed in this report).

I realized crystallization trials and obtained two interesting conditions that I tried to optimise. On the Table 10, as well as in Figure 25, it is shown KLC1_#1 crystallization conditions where crystals and microcrystals were found.

Table 10 - Crystallization conditions found to KLC1_#1. To be optimised.

| Correspondent on Figure 25 | KLC1_#1 Precipitant conditions | Temperature (ºC) |
|---|---|---|
| A, B | 0.1 M Citric Acid pH 5.0, 1.6 M $AMSO_4$ | 17 |
| C | 0.2 M K Fluoride, 2.2 M $AMSO_4$ | |

Until the moment, it was considered that KLC1_#1 crystallization condition (0.1M Citric Acid pH 5.0, 1.6 M $AMSO_4$) should be firstly optimised, due to the crystal formation (Figure 25 A, B). Using Methylene Blue Solution (IZIT Crystal Dye), it was proved (by the entrance of methylene blue into the crystal) that this condition allows to achieve protein crystals and not salt crystals (Figure 25B). Currently, laboratory is working on optimising this crystallization condition, but also the second one (Figure 25C) should be taken in consideration in the near future.

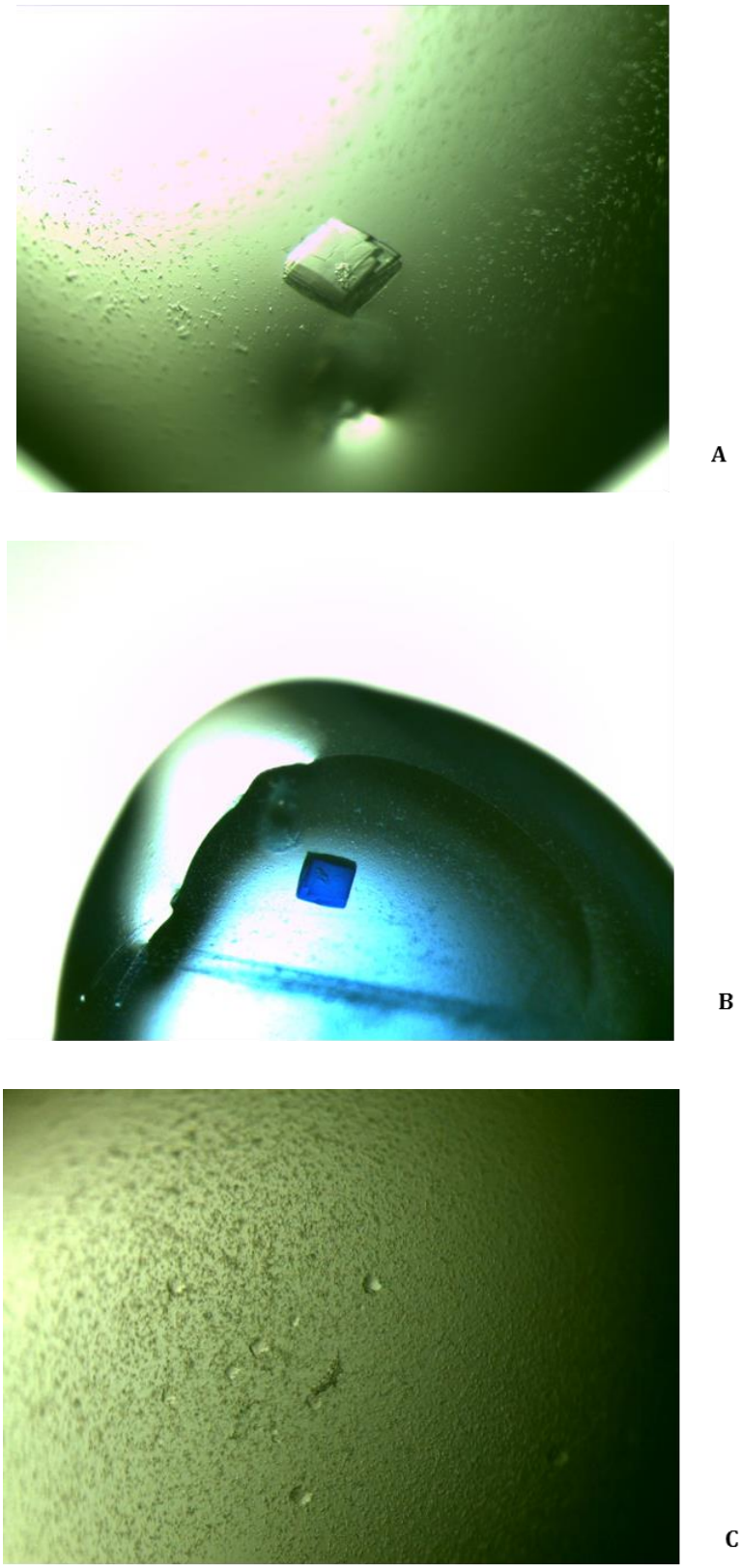


Figure 25 – KLC_#1 crystallization conditions where crystals and microcrystals were found. A - Protein crystal from the condition 0.1 M Citric Acid pH 5.0, 1.6 M $AMSO_4$. B – Same protein crystal shown on A, after testing it with IZIT Crystal Dye, confirming that it is a protein crystal, due to its change of color. C - Protein microcrystals from the condition 0.2 M K Fluoride, 2.2 M $AMSO_4$.

# Characterization of the Structural Integrity of JIP3_LZII

**Circular Dichroism assays of JIP3_LZII_#1 and mutants -** Concerning the secondary structure prediction of JIP3_LZII_#1 and its mutants (fragments designed with 78 residues), circular dichroism was realized. Figure 26 shows the CD spectrum of JIP3_LZII_#1, where this profile clearly demonstrates that this fragment possesses alpha-helix structure.

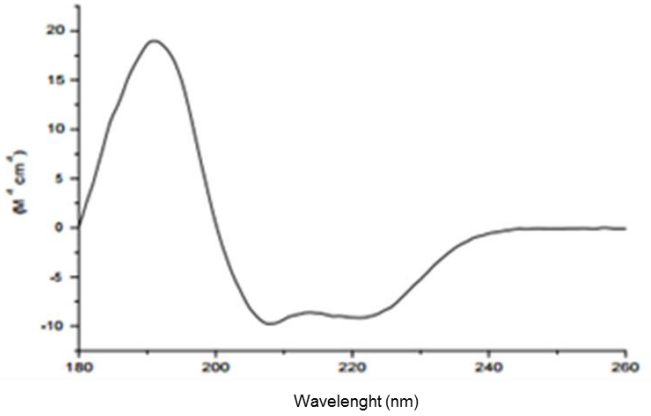


Figure 26 - CD spectrum of JIP3_LZII_#1.

It is possible to determine if these mutations are affecting or not their secondary structure. Results were very conclusive and validated by two different calculation methods. The major sequence part (70-80%) of the JIP3_LZII fragments is folded as alpha-helix, corresponding to 54-62 residues of the fragments. In fact, evidences are in agreement with the theoretically previewed. JIP3_LZIIs conceived possess an N-terminal linker (containing 11 residues where the WW motif is located) which is not belongs to LZII domain. We could assume that the entire LZII domain (67 residues) is correctly folded, as alpha-helix. Only JIP3_LZII_#7 (measured two independent times – 1 and 2) shows no alpha-helix as significant part of the protein fragment. Therefore, it is concluded by CD experiments that this point mutation modifies the secondary structure of the overall protein (low alpha-helix structure percentage prediction, around 35%, which corresponds to 27 residues).Theoretically, the interaction KLC1:JIP3_LZII_#7 should be affected. On Figure 27, it is shown a graphic with the results for all JIP3_LZII fragments designed. Values shown on Figure 27 are present also on Annexe 9.

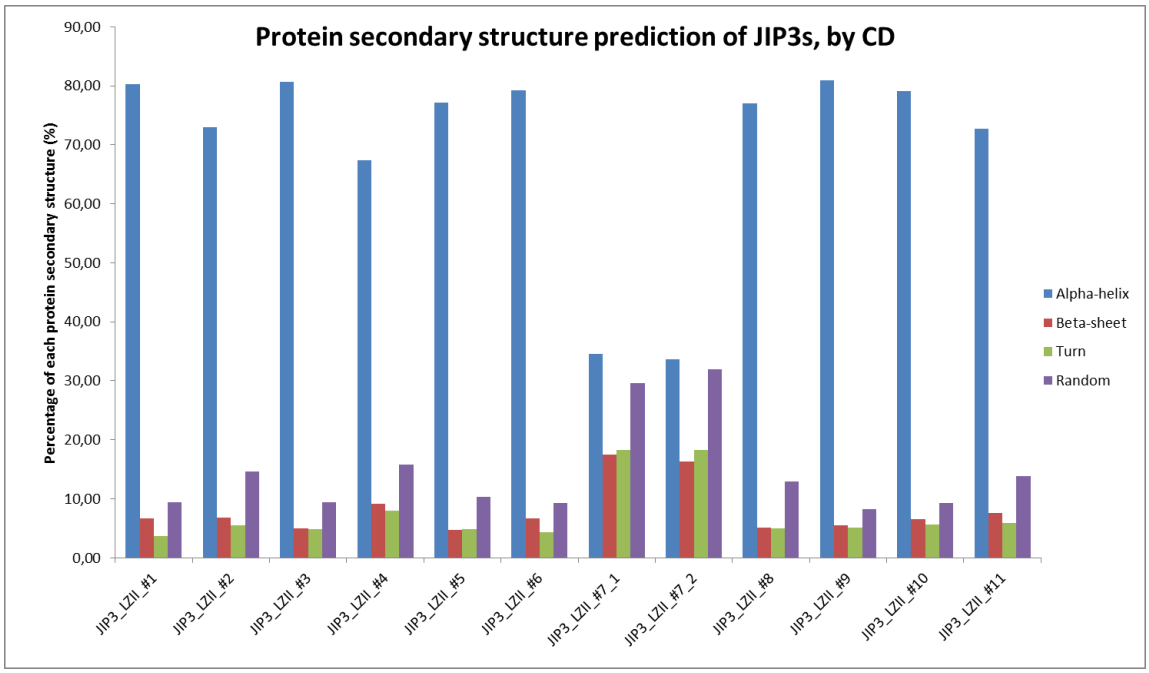


Figure 27 - CD experiments on JIP3_LZII wild type and mutants. It is represented, for each mutant, the percentage of alpha-helix (blue), beta-sheet (red), turns (green) and random conformation (purple). Calculations were performed by an average of CDSSTR (theoretical database software chosen for the case in study) results, obtained from two basis set options (SDP42 and SDP48).

**nano Differential Scanning Fluorimetry assays of JIP3/4_LZII, preliminary studies -** Here, we performed preliminary studies on JIP3/4_LZII mutants using nanoDSF.

JIP3_LZII mutants possess two tryptophan residues (WW motif) in the linker region connecting to the GST tag; after removal of the GST-tag with rTEV protease, the WW motif remains with JIP3_LZII. JIP4_LZII was also conceived with WW motif. Furthermore, as we expect all JIP3/4_LZII fragments to be dimer coiled-coils, WW motif from each monomer should face together and dissociation of the dimer during denaturing process should give significant tryptophan fluorescence signal. This methodology could be applied for JIP3/4_LZII mutants. The presence of Tween 20, detergent which stabilizes the hydrophobic regions of JIP3/4_LZII fragments, would not affect the results on these assays.

Firstly, we performed these experiments with a JIP3_LZII mutant (JIP3_LZII_#10, with a buffer screening – Figure 28 and Annexe 6) in order to understand if it could be possible to achieve the expected results. We confirmed optimal fluorescence signal by one defined peak in each condition, probably due to the dimer dissociation. In this assay, we obtained melting temperatures in the order of 30º-35ºC. Probably these values are in agreement with low stability of JIP3_LZII.

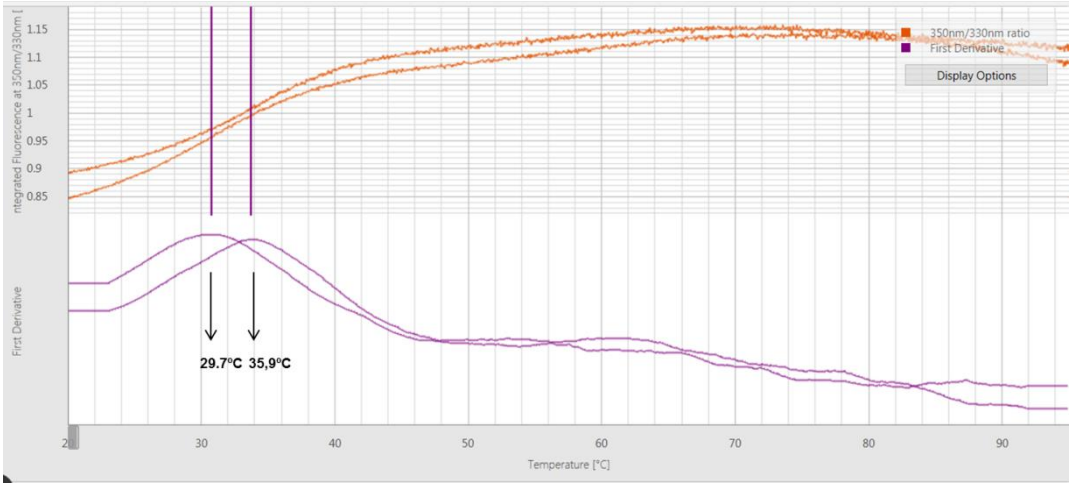


Figure 28 – Two measures of the first nanoDSF assays, using JIP3_LZII_#10. It is shown two of the melting temperatures obtained.

Afterwards, we compared dimer stabilities between JIP3_LZII_#1 and JIP4_LZII_#1, as well as between JIP3_LZII mutants, in the buffer conditions used in other experiments (Annexe 6). The obtained results are an indication of the stability (Kd of dimerization) for JIP3/4_LZII mutants, tested on three different buffer conditions and a fourth condition of refreeze and thaw the proteins in study.

To the case of JIP3_LZII_#1 and JIP4_LZII_#1, it is shown that, for each condition, JIP4_LZII fragment has a melting temperature around 20ºC higher than JIP3_LZII_#1, with 55ºC of melting temperature value. Therefore, even without validation, we can predict that JIP4_LZII_#1 fragment is more stable than JIP3_LZII_#1 (Figure 29). Of note, JIP3_LZII_#1 and JIP4_LZII_#1 have the same limit size, same sequence at the N-terminus after cleavage and both are wild type.

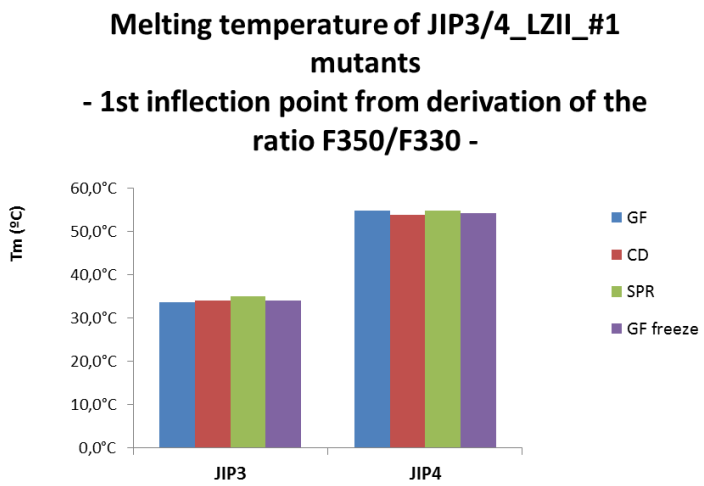


Figure 29 - NanoDSF assays using JIP3_LZII_#1 and JIP4_LZII_#1 fragments. Melting temperatures were calculated, based on the first inflection point from derivation of the ratio F350/F330. Different buffer conditions were tested. GF – gel filtration and storage buffer; CD – circular dichroism buffer; SPR – surface plasmon resonance buffer; GF freeze – same GF buffer, after refreeze and thaw proteins.

Finally, we also realized experiments for JIP3_LZII mutants. On Figure 30, it is represented the overall results in each buffer condition tested on JIP3s (GF - gel filtration and storage buffer; CD – circular dichroism buffer; SPR - Surface Plasmon Resonance buffer (experiments mentioned on Discussion chapter); GF freeze – gel filtration buffer conditions after a second protein thaw). All tested buffers are described on Annexe 6.

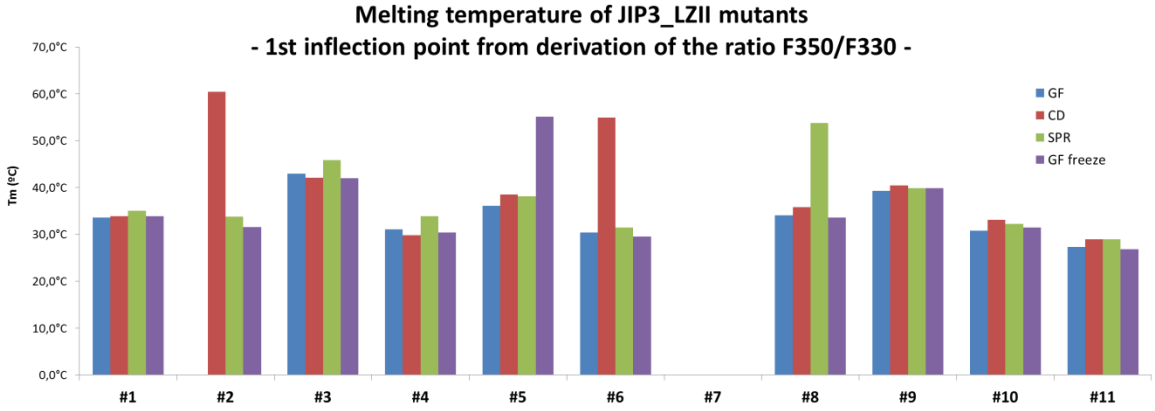


Figure 30 – nanoDSF experiments using JIP3_LZII wild type and mutants. Melting temperatures were calculated, based on the first inflection point from derivation of the ration F350/F330. Different buffer conditions were tested. GF – gel filtration and storage buffer; CD – circular dichroism buffer; SPR – surface plasmon resonance buffer; GF freeze – same GF buffer, after refreeze and thaw proteins.

Interestingly, it is shown for all mutants that their first refreeze and thaw do not affect the protein stability. Results have to be refined but this is an indication that we

could perform a refreeze and thaw during the manipulation of these proteins. However, we could not assume that protein stability would be maintained after several refreeze and thaw moments.

Globally, it is demonstrated that JIP3_LZII mutants possess melting temperatures between 30º-40ºC. Therefore, JIP3s' dimer stability would not be high (to be validated). In order to distinguish precisely the importance of the buffer conditions for each JIP3_LZII mutant, as well as to eliminate measure errors and some significant differences (as shown for the first JIP3 LZII mutant, i.e.), triplicate measures will be performed. It is also shown that for JIP3_LZII_#7, there are no melting temperatures registered in any buffer conditions. Consequently, it is predicted that JIP3_LZII_#7 possesses an incorrect protein folding, in comparison with other JIP3_LZII fragments.

**SEC-MALS experiments of JIP3_LZII_#1 and mutants -** SEC-MALS was realized for JIP3_LZII wild type and its mutants, aiming the knowledge of their oligomeric state, on similar buffer conditions of KLC1:JIP3_LZII interaction experiments performed by SPR assays (performed by P. Llinas, not shown in this manuscript). However, experiments failed, due to the presence of Tween 20 micelles during protein elution, as well as protein aggregation during the experiments. Column choice and buffer conditions (with emphasis on detergent concentration) are currently in optimisation.

**Protein Crystallization assays of JIP3_LZII wild type and mutants – High Throughput Crystallisation Laboratory (HTX) collaboration -** Crystallization Assays were performed with JIP3_LZII wild type and mutants on the HTX platform, Grenoble, France, in order to determine the 3D structure of the LZII domain of JIP3s. The aim to gain such structural information is to visualize if the JIP3_LZII wild type and/or mutants are parallel or anti-parallel coiled-coils, as well as the oligomerization state of the proteins. We expected that JIP3_LZII fragment exhibits dimeric parallel coiled-coil structure. However, recent structural data obtained in the lab suggest that this assumption could be wrong (Llinas et al., submitted).

All JIP3_LZII wild type and mutants (11 proteins) were tested, as described on Materials and Methods, and some crystallization conditions were found as good for optimisation. There are microcrystals and crystal ursins in three conditions, with three different mutants, whose crystallization conditions will be optimised. On the Figure 31, it is shown photos from mentioned microcrystals. Also, on Table 11, JIP3_LZII fragments crystallized, precipitant conditions used and incubation temperatures are shown.

Table 11 - Crystallization conditions of JIP3_LZII mutants.

| Correspondent on Figure 31 | JIP3_LZII mutant | Precipitant conditions to optimize | Temperature (ºC) |
|---|---|---|---|
| A, B | JIP3_LZII_#4 | 0.1 M tri-sodium citrate pH 5.6; 2.5 M 1.6-hexanediol | 4 |
| C | JIP3_LZII_#4 | 0.2 M sodium chloride; 0.1 M sodium acetate pH 4.6; 30 %(v/v) MPD | 20 |
| D | JIP3_LZII_#3, JIP3_LZII_#5 | 0.2 M magnesium formate | 20 |

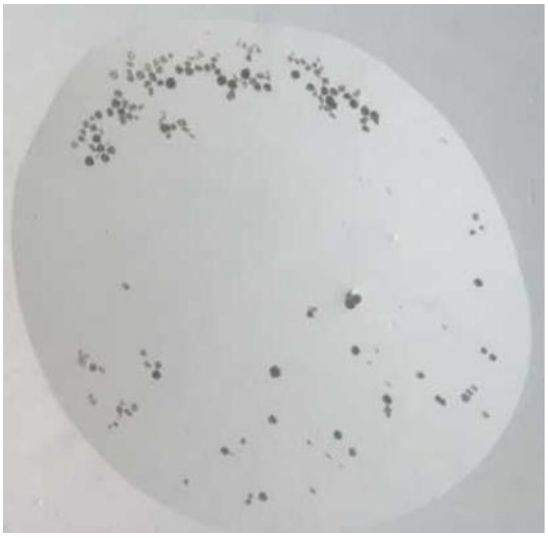

**A**

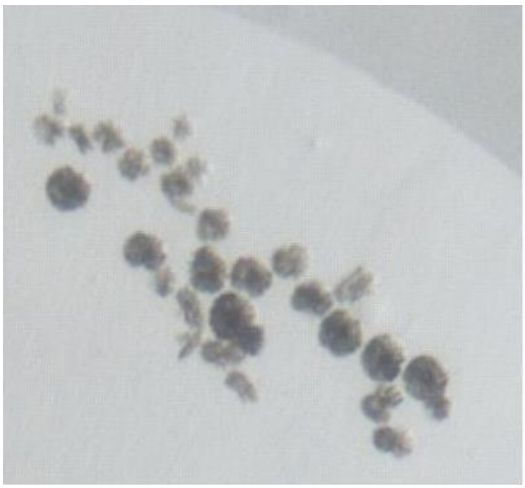

B

C

D

Figure 31 - JIP3_LZII crystallization conditions with the presence of microcrystals. To be optimised, in collaboration with HTX platform, Grenoble, France. Conditions shown on A, B, C and D are described on Table 11. B – Zoom picture of A, showing microcrystals with higher detail.

# Protein-Protein interaction Characterization

**KLC1_#0 and JIP4_LZII_#1, MST preliminary studies -** Here, it is presented preliminary studies of KLC1_#0:JIP4_LZII_#1 interaction, by MST. Buffer optimisations were performed and, therefore, only best results achieved are shown. In these experiments, JIP4_LZII_#1 was used due to its high homology with JIP3_LZII, but also because of JIP4_LZII initial quantity required to perform MST, less expensive and easier to achieve, in comparison with JIP3_LZII mutants. JIP4_LZII_#1 had higher purification yields than JIP3_LZII mutants (not shown); thus, JIP4_LZII_#1 would be suitable to these MST assays.

KLC1_#0 was labelled with MO-L002 Monolight Protein Labeling Kit Green-NHS, according with Nanotemper protocols.

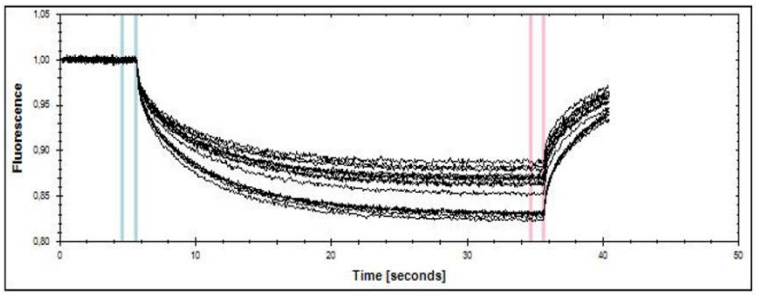


A

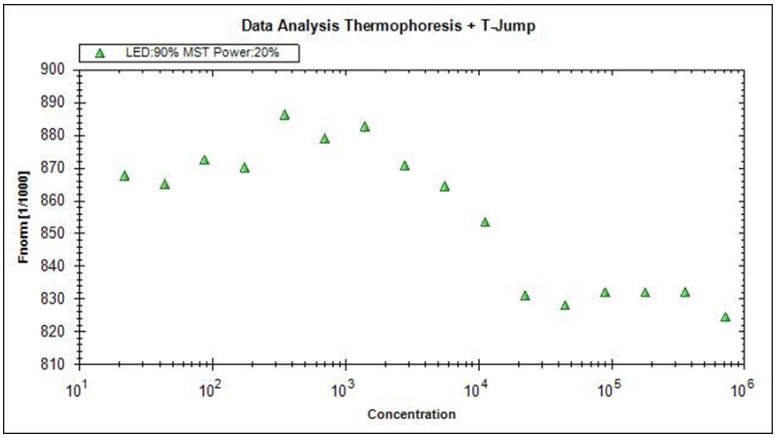


B

Figure 32 – MST experiments using labeled-KLC1_#0 and JIP4_LZII_#1. It is shown the results for each one of the 16 capillaries tested, corresponding to 16 different JIP4 dilutions, all in the presence of the same quantity of KLC1-labeled. A – Graphic showing the variation of fluorescence detected, in function of time. B – Thermophoresis and T-Jump data analysis.

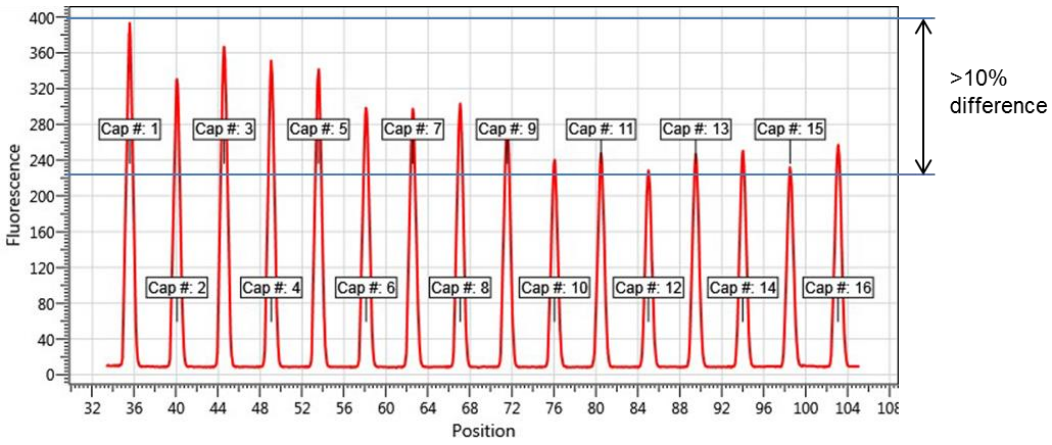


Figure 33 – Capillary Scan from MST experiments of labelled-KLC1 and JIP4_LZII. As it is evidenced by the graphic, the difference between initial fluorescence values of the capillaries is higher than 10%. Therefore, results could not be validated.

As shown on Figure 32, an interaction was detected between labeled-KLC1_#0 and JIP4_LZII_#1. No protein aggregation was found during the experiments, along all the dilutions tested (confirmed by the graphic profile on Figure 32A). At the same time, on Figure 32B, it is exposed the existence of an inflection zone (between $10^3$ and $10^5$ of JIP4_LZII_#1 concentration (nano molar)), revealing the interval where the Kd of this interaction could be calculated. However, as indicated on Figure 33, the Capillary Scan made before the measurements showed a huge fluorescence difference between capillaries. Usually, in order to correctly calculate Kd values, the capillary scan should present fluorescence differences no higher than 10%, between them. Here, maybe there were protein adsorption to Standard Capillaries, or buffer conditions should be optimised for the complex.

Therefore, it was not possible to validate a Kd value for the complex, but it was confirmed an interaction with a Kd in the order of 0.5 uM.

# Discussion and Future Perspectives

In the course of this project, we aim to characterize, from a structural perspective, the recruitment of JIP3/4_LZII by KLC1_TPR domain of kinesin1. To realize it, we intend to understand how the complex interaction takes place, obtaining structural and biophysical information of the complex, as well as knowledge about each JIP3/4_LZII and KLC1 interfaces. Based on a molecular docking performed by our collaborators, we purpose to identify and confirm regions and residues involved in the complex interaction. Before my arrival in the group, KLC1 interface was already investigated and validated (Phase1). Also, JIP3_LZII expression vectors were previously conceived. During my Master's Project, I mainly participated on JIP3/4_LZII interface investigation (Phase 2). Thus, to be handled for complex interaction experiments, several JIP3_LZII mutants, as well as new KLC1 fragments and mutants, were successfully produced and their structural integrity checked. I also participated on preliminary experiments to determine the 3D structure determination of the KLC1:JIP3/4_LZII complex by SAXS (Phase 3, not developed in this manuscript). Concerning the main objectives of the study, very positive advancements were achieved.

JIP3_LZII mutants were conceived in order to identify which residues of JIP3_LZII are involved in KLC1 interaction. To realize it, affinity binding experiments between KLC1 and JIP3_LZII mutants were performed using MST and SPR. However, in order to correctly describe these data, it is important to make sure that JIP3_LZII mutants produced are well folded. Indeed, if JIP3_LZII mutants are badly folded due to the mutation designed, interaction with KLC1 could be prevented. Therefore, one of my main objectives was to investigate the structural integrity of the JIP3_LZII mutants. Hence, I performed CD experiments in order to evaluate the secondary structure composition of each JIP3_LZII mutant. JIP3_LZII is a leucine zipper coiled-coil which folds as an alpha-helical protein. CD experiments predicted an average of alpha-helix structure around 80%, for almost of JIP3_LZII mutants. Accordingly with their protein sequence, (JIP3_LZII_#1 shown on Annexe 7), we assumed that all leucine zipper regions of the protein fragments designed have their secondary structure correctly folded, as alpha-helix domains. Indeed, after GST-tag cleavage, JIP3_LZII fragment is fused at their N-terminus to the remaining part of the rTEV cleavage site that should not adopt helical folding. Furthermore, JIP3 fragments possess 78 residues, where 11 residues are outside the LZII, on the N-terminus. By the CD results, we could predict that 62 residues (80% of the protein sequence) are coiled-coil folded, near from 67 residues which are a part of the LZII domain conceived. However, CD experiments

showed also that JIP3_LZII_#7 mutant is different with huge differences on its secondary structure composition, as shown on Figure 27. The JIP3_LZII_#7 mutant has alpha-helix percentage prediction around 34% in contrast to the 80% for other mutants. Thus, we considered that this mutation in JIP3_LZII prevents its correct (expected) folding. To conclude, affinity binding experiment between this JIP3_LZII mutant and KLC1 could not be correctly described and they will be removed from the study. Interestingly, as shown on Table 5, this mutant has the lowest purification yield during its protein expression on bacterial systems, comparing with other mutants. This difference could be due to a lower stability of the protein maybe caused by its incorrect folding.

In parallel to CD experiments, I also performed nanoDSF assays in order to evaluate the stability of the JIP3_LZII mutants. NanoDSF approach allows to evaluate the heat denaturation curve of proteins following intrinsic tryptophan fluorescence. The JIP3_LZII fragments by their own possess no aromatic residues, but the construction of JIP3_LZII was conceived with a double tryptophan (WW) motif inserted between the protease cleavage site and the protein. Therefore, after GST-tag removal, two tryptophans are present at the N-terminus of the LZII. If we consider that JIP3_LZII coiled-coil is parallel, as expected by previous structural studies (Isabet T., et al., 2009), there would have, at the N-terminus of the dimer, a patch of 4 tryptophan residues, two on each monomer, facing together. We anticipated that during heat denaturation process, dimer dissociation should produce a strong intrinsic tryptophan fluorescence signal. For all the JIP3_LZII mutants, except JIP3-LZII_#7, the Tm is relatively similar. The average Tm is around 30-35°C, which is unexpectedly low. Interestingly, no melting temperature could be determined for JIP3_LZII_#7 mutant. Therefore, it is not possible to achieve a heat denaturation profile for this mutant. In fact, this is in agreement with CD experiment results, and together, these elements support the conclusion that JIP3_LZII_#7 is not well folded and, thus, not stable. This data also confirms that JIP3_LZII_#7 should not be able to interact with KLC1 and will not be taken in account in our interpretation of affinity binding experiments. In conclusion, except for the JIP3_LZII_#7 mutant, we have evidences that all other JIP3_LZII mutants are well folded and could be used on interaction experiments.

Finally, because a previous structural study in the group has allowed to crystallize a truncated form of JIP3_LZII (missing the 2 first heptad repeats) in an anti-parallel arrangement, we are wondering if the full wild type JIP3_LZII or the mutants studied here adopt parallel or anti-parallel arrangement. To answer this question, I have taken the advantage of having the wild type and several mutants of the full

JIP3_LZII fragment produced and purified to perform crystallization assays, increasing the chance to find a crystal packing. Crystals were obtained for several mutants and should be reproduced and improved in the lab in order to solve the 3D structure.

Affinity binding experiments were performed to study KLC1:JIP3/4_LZII mutant interaction using SPR and MST. On the one hand, SPR experiments that have been done by P. Llinas in the group (in coll. Institut Pasteur) revealed that two mutants on the heptad 4 of JIP3_LZII prevent the interaction with KLC1, while the others only slightly affect the interaction. SPR results are not extensively developed in the manuscript. However, it is affirmed the use of the protein fragments produced during the project were successfully used during these experiments. In order to confirm these results, we will perform MST experiments. I performed (with P. Llinas) preliminary MST experiments, which confirm a Kd value of the complex KLC1_#0:JIP4_LZII_#1 in the range of micro Molar, as previously reported (Quyen et al., 2005 and SPR data). This result confirms that MST could be used to perform affinity binding experiments, which will be done in the near future. In conclusion of this part, Phase 2 (JIP3 interface validation) has to be reinforced with new JIP3_LZII mutants, which are now in preparation. Indeed, on the first part of Phase 2, point mutations were performed on the second, third and fourth heptad repeats of JIP3_LZII. Relevant point mutations found by SPR, affecting the formation of the complex, are positioned on the fourth heptad of JIP3_LZII. Therefore, with the aim of a deeply understanding of JIP3_LZII interface, a second group of protein mutants were planned to be conceived (part 2 of Phase 2). More point mutations will be performed on the fifth and sixth heptad, to better delimit the interaction zone of JIP3_LZII with KLC1. Furthermore, it will be arranged another group of mutants on the interaction zone (third and fourth heptads) to clarify and confirm JIP3_LZII interacting residues. Double mutation protein constructs will be also designed, in order to validate JIP3_LZII interface. After JIP3 new mutants' conception, protein production will be made, following same optimised protocols during this project. At the same manner, JIP3_LZII characterization will be performed and completed to all new mutants, allowing the knowledge of their structural integrity (by CD, nanoDSF and SEC-MALS). Afterwards, binding assays will be performed by MST and SPR with new JIP3_LZII mutants and KLC1_#1, but also handling with KLC1_#2, not yet tested.

In order to complement the site-directed mutagenesis and affinity binding studies (phases 1 and 2) to validate the KLC:JIP3_LZII docking model, the low

resolution 3D structure of the complex will be determined using SAXS (phase 3). I participated to the SAXS experiment (with P. Llinas) at the SWING beamline of the SOLEIL synchrotron, helping to collect preliminary but encouraging data for the complex. SAXS results are not extensively developed in the manuscript. However, it is affirmed the use of the protein fragments produced during the project was successfully used during experiments. These experiments are currently under optimisation.

The finalization of this project (new JIP3_LZII mutant production, SPR and MST assays, as well as SAXS experiments) will be a part of my PhD, which I will do in the group of Julie Ménétrey, at the “Institut de Biologie Intégrative de la Celulle”, joining the University of Paris-Saclay, at the doctoral school “Innovation Thérapeutique, du fondamental à l’appliqué”. In addition, I will realize the structural characterization of JIP3_LZI recruitment by the tail of KHC chain, from kinesin1 that correspond to the second mode of binding of JIP3/4 by Kinesin-1. Altogether, these two studies will allow to gain a full picture of how JIP3/4 proteins are recruited and transported by kinesin1, as well as their association with protein MAPK cascades in neurons.

# Bibliography

Adio, S., J. Reth, F. Bathe and G. Woehlke (2006). "Review: regulation mechanisms of Kinesin-1." J Muscle Res Cell Motil **27**(2): 153-160.

Bowman, A. B., A. Kamal, B. W. Ritchings, A. V. Philp, M. McGrail, J. G. Gindhart and L. S. Goldstein (2000). "Kinesin-dependent axonal transport is mediated by the sunday driver (SYD) protein." Cell **103**(4): 583-594.

Cavalli, V., P. Kujala, J. Klumperman and L. S. Goldstein (2005). "Sunday Driver links axonal transport to damage signaling." The Journal of cell biology **168**(5): 775-787.

De Vos, K. J., A. J. Grierson, S. Ackerley and C. C. Miller (2008). "Role of axonal transport in neurodegenerative diseases*." Annu. Rev. Neurosci. **31**: 151-173.

DeBoer, S. R., Y. You, A. Szodorai, A. Kaminska, G. Pigino, E. Nwabuisi, B. Wang, T. Estrada-Hernandez, S. Kins and S. T. Brady (2008). "Conventional Kinesin Holoenzymes Are Composed of Heavy and Light Chain Homodimers†." Biochemistry **47**(15): 4535-4543.

Foth, B. J., M. C. Goedecke and D. Soldati (2006). "New insights into myosin evolution and classification." Proc Natl Acad Sci U S A **103**(10): 3681-3686.

Gerdes, J. M., E. E. Davis and N. Katsanis (2009). "The vertebrate primary cilium in development, homeostasis, and disease." Cell **137**(1): 32-45.

Gindhart, J. G. (2006). "Towards an understanding of kinesin-1 dependent transport pathways through the study of protein-protein interactions." Brief Funct Genomic Proteomic **5**(1): 74-86.

Gunawardena, S. and L. S. Goldstein (2001). "Disruption of axonal transport and neuronal viability by amyloid precursor protein mutations in Drosophila." Neuron **32**(3): 389-401.

Hammond, J. W., K. Griffin, G. T. Jih, J. Stuckey and K. J. Verhey (2008). "Co-operative Versus Independent Transport of Different Cargoes by Kinesin-1." Traffic **9**(5): 725-741.

Hirokawa, N. (1998). "Kinesin and dynein superfamily proteins and the mechanism of organelle transport." Science **279**(5350): 519-526.

Hirokawa, N., S. Niwa and Y. Tanaka (2010). "Molecular motors in neurons: transport mechanisms and roles in brain function, development, and disease." Neuron **68**(4): 610-638.

Hirokawa, N., Y. Noda, Y. Tanaka and S. Niwa (2009). "Kinesin superfamily motor proteins and intracellular transport." Nature reviews Molecular cell biology **10**(10): 682-696.

Hirokawa, N. and R. Takemura (2005). "Molecular motors and mechanisms of directional transport in neurons." Nat Rev Neurosci **6**(3): 201-214.

Isabet, T., G. Montagnac, K. Regazzoni, B. Raynal, F. El Khadali, P. England, M. Franco, P. Chavrier, A. Houdusse and J. Ménétrey (2009). "The structural basis of Arf effector specificity: the crystal structure of ARF6 in a complex with JIP4." The EMBO journal **28**(18): 2835-2845.

Kaan, H. Y. K., D. D. Hackney and F. Kozielski (2011). "The structure of the kinesin-1 motor-tail complex reveals the mechanism of autoinhibition." Science **333**(6044): 883-885.

Karki, S. and E. L. Holzbaur (1999). "Cytoplasmic dynein and dynactin in cell division and intracellular transport." Curr Opin Cell Biol **11**(1): 45-53.

Kelkar, N., S. Gupta, M. Dickens and R. J. Davis (2000). "Interaction of a mitogen-activated protein kinase signaling module with the neuronal protein JIP3." Molecular and cellular biology **20**(3): 1030-1043.

Kelkar, N., C. L. Standen and R. J. Davis (2005). "Role of the JIP4 scaffold protein in the regulation of mitogen-activated protein kinase signaling pathways." Molecular and cellular biology **25**(7): 2733-2743.

Lippincott-Schwartz, J., N. B. Cole, A. Marotta, P. A. Conrad and G. S. Bloom (1995). "Kinesin is the motor for microtubule-mediated Golgi-to-ER membrane traffic." The Journal of cell biology **128**(3): 293-306.

Lupas, A., M. Van Dyke and J. Stock (1991). "Predicting coiled coils from protein sequences." Science **252**(5009): 1162-1164.

Morrison, D. K. and R. J. Davis (2003). "Regulation of map kinase signaling modules by scaffold proteins in mammals*." Annual review of cell and developmental biology **19**(1): 91-118.

Nguyen, Q., C. M. Lee, A. Le and E. P. Reddy (2005). "JLP associates with kinesin light chain 1 through a novel leucine zipper-like domain." Journal of Biological Chemistry **280**(34): 30185-30191.

Santama, N., P. Connie, L.-L. Ong and H. Yu (2004). "Distribution and functions of kinectin isoforms." Journal of cell science **117**(19): 4537-4549.

Schnapp, B. J. (2003). "Trafficking of signaling modules by kinesin motors." Journal of cell science **116**(11): 2125-2135.

Vale, R. D. (2003). "The molecular motor toolbox for intracellular transport." Cell **112**(4): 467-480.

Vale, R. D. (2003). "The molecular motor toolbox for intracellular transport." Cell **112**(4): 467-480.

Verhey, K. J., D. Meyer, R. Deehan, J. Blenis, B. J. Schnapp, T. A. Rapoport and B. Margolis (2001). "Cargo of kinesin identified as JIP scaffolding proteins and associated signaling molecules." The Journal of cell biology **152**(5): 959-970.

Watt, D., R. Dixit and V. Cavalli (2015). "JIP3 activates kinesin-1 motility to promote axon elongation." Journal of Biological Chemistry: jbc. M115. 651885.

Whitmarsh, A. (2006). "The JIP family of MAPK scaffold proteins." Biochemical Society Transactions **34**(Pt 5): 828-832.

Woźniak, M. J. and V. J. Allan (2006). "Cargo selection by specific kinesin light chain 1 isoforms." The EMBO journal **25**(23): 5457-5468.

Yasuda, J., A. J. Whitmarsh, J. Cavanagh, M. Sharma and R. J. Davis (1999). "The JIP group of mitogen-activated protein kinase scaffold proteins." Molecular and cellular biology **19**(10): 7245-7254.

Zhu, H., H. Y. Lee, Y. Tong, B.-S. Hong, K.-P. Kim, Y. Shen, K. J. Lim, F. Mackenzie, W. Tempel and H.-W. Park (2012). "Crystal structures of the tetratricopeptide repeat domains of kinesin light chains: insight into cargo recognition mechanisms." PloS one **7**(3); 03, 2012).

# Annexes

Annexe 1 - Composition and use of Loading Buffer 5x.

| **Loading Buffer x5** | |
|---|---|
| *Composition* | *How to use* |
| 0.06 M Tris-HCl pH 6.8<br>4% SDS<br>25% Glycerol<br>5% β-Mercaptoethanol<br>0.1 % w/v Bromophenol blue | Proteins were previously mixed with loading buffer, at final concentration of 1x. Thus protein samples were denatured by heat, at 95ºC. |

Annexe 2 - Stacking and Runnung Compositions of SDS-PAGE.

| **SDS-PAGE Composition** | |
|---|---|
| *Stacking gel* | *Running Gel* |
| 15% PolyAcrylamide<br>0.44 M Tris-HCl pH 8.8<br>0.2% SDS<br>0.1% TEMED<br>0.1 % AMPS | 4% PolyAcrylamide<br>0.09 M Tris-HCl pH 6.8<br>0.2% SDS<br>0.1% TEMED<br>0.1 % AMPS |

Annexe 3 - Buffer conditions optimised and used during Solubility and Minipurification tests.

| | **Buffer conditions used on Solubility and Minipurification tests** |
|---|---|
| **Buffer's funtion** | *KLC1 fragments* |
| **Lysis** | 50 mM Hepes pH 8.0, 500 mM NaCl, 5 mM Imidazole pH 7.0, 10% Glycerol |
| **Wash** | 50 mM Hepes pH 8.0, 500 mM NaCl, 5 mM Imidazole pH 7.0, 10% Glycerol |
| **Elution** | 50 mM Hepes pH 8.0, 500 mM NaCl, 250 mM Imidazole pH 7.0, 10% Glycerol |
| | *JIP3_LZII_#1* |
| **Lysis** | 50 mM Tris pH 8.0, 250 mM NaCl, 1 mM EDTA, 5 mM MgCl2, 10% Glycerol |
| **Wash** | 50 mM Tris pH 8.0, 250 mM NaCl, 1 mM EDTA, 5 mM MgCl2, 10% Glycerol |
| **Elution** | 50 mM Tris pH 8.0, 250 mM NaCl, 10 mM Reduced-Glutathione, 1 mM EDTA, 5 mM MgCl2, 10% Glycerol |

Annexe 4 - Protein Purification Buffers of KLC1 and JIP3_LZII fragments.

| Chromatography Purification Step | Buffer's name/function | Buffer conditions used on KLC1 fragments Purification |
|---|---|---|
| His-trap Affinity | Lysis | 25 mM Hepes pH 8.0, 500 mM NaCl, 5 mM Imidazole pH 8.0, 10% Glycerol |
| | Wash | 50 mM Hepes pH 8.0, 500 mM NaCl, 20 mM Imidazole pH 8.0, 5% Glycerol |
| | Elution | 50 mM Hepes pH 8.0, 500 mM NaCl, 500 mM Imidazole pH 8.0, 5% Glycerol |
| Size Exclusion | Gel filtration and storage | 50 mM Hepes pH 8.0, 200 mM NaCl |

| Chromatography Purification Step | Buffer's name/funtion | Buffer conditions used on JIP3_LZII fragments Purification |
|---|---|---|
| 1st GST-trap Affinity | Lysis | 50 mM Tris pH 8.0, 1 M NaCl, 1 mM EDTA, 5 mM MgCl2, 10% Glycerol, 0.05% Tween 20 |
| | Wash | 50 mM Tris pH 8.0, 1 M NaCl, 1 mM EDTA, 5% Glycerol, 0.05% Tween 20 |
| | Elution | 50 mM Tris pH 8.0, 1 M NaCl, 1 mM EDTA, 10 mM Reduced-Glutathione, 5% Glycerol, 0.05% Tween 20 |
| His-trap Affinity | His-buffer A | 50 mM Tris pH 8.0, 1 M NaCl, 5% Glycerol, 0.05% Tween 20 |
| | His-buffer B | 50 mM Tris pH 8.0, 1 M NaCl, 500 mM Imidazole 5% Glycerol, 0.05% Tween 20 |
| 2nd GST-trap Affinity | GST-buffer A | 50 mM Tris pH 8.0, 1 M NaCl, 5% Glycerol, 0.05% Tween 20 |
| | GST-buffer B | 50 mM Tris pH 8.0, 1 M NaCl, 10 mM Reduced-Glutathione 5% Glycerol, 0.05% Tween 20 |
| Size Exclusion | Gel filtration and storage | 50 mM Tris pH 8.0, 150 mM NaCl, 0.05% Tween 20 |

Annexe 5 - Buffer Conditions analysed on KLC1 fragments, by TSA. Secondly , Tm values of TSA experiments for KLC1_#1 and KLC1_#3.

| TSA Conditions analysed on KLC1 fragments | | | | |
|---|---|---|---|---|
| **TSA Condition** | **Buffer Conditions** | **NaCl / mM** | **KCL / mM** | **TCEP / mM** |
| 1 | 50 mM Acetate pH 5.0 | - | - | - |
| 2 | | 50 | - | - |
| 3 | | 200 | - | - |
| 4 | | 500 | - | - |
| 5 | | 200 | - | 10 |
| 6 | | - | 200 | - |
| 7 | 50 mM MES pH 6.0 | - | - | - |
| 8 | | 50 | - | - |
| 9 | | 200 | - | - |
| 10 | | 500 | - | - |
| 11 | | 200 | - | 10 |
| 12 | | - | 200 | - |
| 13 | 50 mM HEPES pH 7.0 | - | - | - |
| 14 | | 50 | - | - |
| 15 | | 200 | - | - |
| 16 | | 500 | - | - |
| 17 | | 200 | - | 10 |
| 18 | | - | 200 | - |
| 19 | 50 mM Tris pH 8.0 | - | - | - |
| 20 | | 50 | - | - |
| 21 | | 200 | - | - |
| 22 | | 500 | - | - |
| 23 | | 200 | - | 10 |
| 24 | | - | 200 | - |
| 25 | 50 mM Glycine pH 9.0 | - | - | - |
| 26 | | 50 | - | - |
| 27 | | 200 | - | - |
| 28 | | 500 | - | - |
| 29 | | 200 | - | 10 |
| 30 | | - | 200 | - |

| TSA Buffers Tested | KLC1_#1 | | KLC1_#3 | |
|---|---|---|---|---|
| | Tm /ºC | s | Tm /ºC | s |
| 1 | 41,43 | 0,75 | 74,51 | 0,43 |
| 2 | 42,04 | 0,87 | 72,12 | 0,38 |
| 3 | 39,71 | 3,09 | 69,4 | 0,62 |
| 4 | 41,6 | 1,18 | 65,84 | 0,85 |
| 5 | Not defined | / | Not defined | / |
| 6 | 38,61 | 4,95 | 68,24 | 0,62 |
| 7 | 49,08 | 3,53 | 76,91 | 1,45 |
| 8 | Not defined | / | 76,25 | 0,5 |
| 9 | 51,46 | 0,18 | 74,59 | 0,14 |
| 10 | 52,23 | 0,1 | 73,69 | 0,57 |
| 11 | Not defined | / | Not defined | / |
| 12 | 50,87 | 0,17 | 73,36 | 0,8 |
| 13 | 45,9 | 0,09 | 81,78 | 0,52 |
| 14 | 52,72 | 0,24 | 81,62 | 0,14 |
| 15 | 55,13 | 0,17 | 81,45 | 0,25 |
| 16 | 58,44 | 0,09 | 81,78 | 0,14 |
| 17 | Not defined | / | Not defined | / |
| 18 | 55,71 | 0,09 | 81,37 | 0,14 |
| 19 | 44,45 | 0,18 | 83,1 | 0,57 |
| 20 | 50,54 | 0,28 | 83,51 | 0,29 |
| 21 | 55,16 | 0,09 | 83,93 | 0,25 |
| 22 | 58,49 | 0,09 | 84,26 | 0,14 |
| 23 | Not defined | / | Not defined | / |
| 24 | 55,61 | 0 | 83,85 | 0,14 |
| 25 | 44,48 | 0,16 | 84,34 | 0,14 |
| 26 | 48,58 | 0,49 | 84,59 | 0,14 |
| 27 | 54,31 | 0,33 | 84,84 | 0,14 |
| 28 | 57,52 | 0,09 | 85 | 0,14 |
| 29 | Not defined | / | Not defined | 0,14 |
| 30 | 54,25 | 0,19 | 84,75 | 0,14 |

Annexe 6 - Buffer conditions analysed on JIP3_LZII_#10, by nanoDSF. Various experiment buffer compositions analysed on JIP3_LZIIs, by nanoDSF.

| nanoDSF Conditions analysed on JIP3_LZII_#10 | | | |
|---|---|---|---|
| **nanoDSF Condition** | **Buffer Conditions** | **Imidazole / mM** | **NaCl / mM** |
| 1 | 25 mM MES pH 6.5 | - | 100 |
| 2 | 25 mM Hepes pH 7.0 | - | |
| 3 | 25 mM Hepes pH 7.5 | - | |
| 4 | 25 mM Tris pH 8.0 | - | |
| 5 | 25 mM MES pH 6.5 | - | 200 |
| 6 | 25 mM Hepes pH 7.0 | - | |
| 7 | 25 mM Hepes pH 7.5 | - | |
| 8 | 25 mM Tris pH 8.0 | - | |
| 9 | 25 mM MES pH 6.5 | - | 300 |
| 10 | 25 mM Hepes pH 7.0 | - | |
| 11 | 25 mM Hepes pH 7.5 | - | |
| 12 | 25 mM Tris pH 8.0 | - | |
| 13 | 25 mM MES pH 6.5 | 50 | 100 |
| 14 | 25 mM Hepes pH 7.0 | | |
| 15 | 25 mM Hepes pH 7.5 | | |
| 16 | 25 mM Tris pH 8.0 | | |
| 17 | 25 mM MES pH 6.5 | | 200 |
| 18 | 25 mM Hepes pH 7.0 | | |
| 19 | 25 mM Hepes pH 7.5 | | |
| 20 | 25 mM Tris pH 8.0 | | |
| 21 | 25 mM MES pH 6.5 | | 300 |

| nanoDSF Buffer Conditions analysed on JIP3_LZII fragments | | |
|---|---|---|
| **Buffer Designation** | **JIP3_LZII Experiments were buffer is used** | **Composition** |
| GF | Size Exclusion Chromatography and JIP3_LZII Storage | 50 mM Tris pH 8.0, 150 mM NaCl, 0.05% Tween 20 |
| CD | Circular Dichroism | 20 mM phosphate pH 7.0, 150 mM NaF, 0.05% Tween 20 |
| SPR | Surface Plasmon Resonance | 25 mM Hepes pH 7.0, 500 mM NaCl, 5 mM MgCl2, 0.05 % Tween 20, 100 uM EDTA |
| GF freeze | Same as GF, after re-freeze and thaw | 50 mM Tris pH 8.0, 150 mM NaCl, 0.05% Tween 20 |

Annexe 7 - KLC1_#1 and JIP3_LZII_#1 protein fragment sequences

| **KLC_#1 protein sequence (His-tagged)** |
| --- |
| MGYEIPARLRTLHNLVIQYASQGRYEVAVPLCKQALEDLEKTSGHDHPDVATMLNILA<br>LVYRDQNKYKDAANLLNDALAIREKTLGKDHPAVAATLNNLAVLYGKRGKYKEAEPLC<br>KRALEIREKVLGKDHPDVAKQLNNLALLCQNQGKYEEVEYYYQRALEIYQTKLGPDDP<br>NVAKTKNNLASCYLKQGKFKQAETLYKEILTRAHEREFGSVDDENKPIWMHAEEREE<br>CKGKQKDGTSFGEYGGWYKACKVDSPTVTTTLKNLGALYRRQGKFEAAETLEEAAM<br>RSRKQGLDNVHENLYFQGLEHHHHHH |
| |
| **JIP3_LZII_#1 protein sequence (GST-tagged)** |
| MSPILGYWKIKGLVQPTRLLLEYLEEKYEEHLYERDEGDKWRNKKFELGLEFPNLPYYI<br>DGDVKLTQSMAIIRYIADKHNMLGGCPKERAEISMLEGAVLDIRYGVSRIAYSKDFETL<br>KVDFLSKLPEMLKMFEDRLCHKTYLNGDHVTHPDFMLYDALDVVLYMDPMCLDAFPK<br>LVCFKKRIEAIPQIDKYLKSSKYIAWPLQGWQATFGGGDHPPKIDTTENLYFQGAMDW<br>WFMGKEVGNLLLENSQLLETKNALNVVKNDLIAKVDQLSGEQEVLRGELEAAKQAKV<br>KLENRIKELEEELKRV |

Annexe 8 – Crystallization Solubility Screening, performed on the laboratory. Usually, we use this screening on crystallization trials protein fragments in study. We aim to obtain information about protein concentration, pH and salt conditions that we could use to achieved protein crystals.

| **Crystallization Solubility Screening, used to KLC1_#1 crystallization assays** | | | | |
|---|---|---|---|---|
| 1.5 M $AMSO_4$ ; 0.1 M MES pH 6.0 | 1.9 M $AMSO_4$ ; 0.1 M MES pH 6.0 | 2.3 M $AMSO_4$ ; 0.1 M MES pH 6.0 | 2.7 M $AMSO_4$ ; 0.1 M MES pH 6.0 | 3.1 M $AMSO_4$ ; 0.1 M MES pH 6.0 |
| 1.5 M $AMSO_4$ ; 0.1 M Tris pH 8.0 | 1.9 M $AMSO_4$ ; 0.1 M Tris pH 8.0 | 2.3 M $AMSO_4$ ; 0.1 M Tris pH 8.0 | 2.7 M $AMSO_4$ ; 0.1 M Tris pH 8.0 | 3.1 M $AMSO_4$; 0.1 M Tris pH 8.0 |
| 15% $KH_2PO_4$ ; 0.1 M MES pH 6.0 | 20% $KH_2PO_4$ ; 0.1 M MES pH 6.0 | 25% $KH_2PO_4$ ; 0.1 M MES pH 6.0 | 30% $KH_2PO_4$ ; 0.1 M MES pH 6.0 | 35% $KH_2PO_4$ ; 0.1 M MES pH 6.0 |
| 15% $KH_2PO_4$ ; 0.1 M Tris pH 8.0 | 20% $KH_2PO_4$ ; 0.1 M Tris pH 8.0 | 25% $KH_2PO_4$ ; 0.1 M Tris pH 8.0 | 30% $KH_2PO_4$ ; 0.1 M Tris pH 8.0 | 35% $KH_2PO_4$ ; 0.1 M Tris pH 8.0 |

Annexe 9 - JIP3_LZII Secondary Structure Prediction values, calculated as described, by CD experiments.

| **Protein Secondary Structure Prediction values, calculated by CD** | | | | | |
|---|---|---|---|---|---|
| **JIP3_LZIIs** | **Helix** | **Strand** | **Turn** | **Random** | **Total** |
| **JIP3_LZII_#1** | **80,30** | **6,70** | **3,75** | **9,45** | **100,20** |
| JIP3_LZII_#2 | 73,00 | 6,85 | 5,45 | 14,65 | 99,95 |
| JIP3_LZII_#3 | 80,70 | 5,00 | 4,80 | 9,40 | 99,90 |
| JIP3_LZII_#4 | 67,35 | 9,10 | 7,95 | 15,80 | 100,20 |
| JIP3_LZII_#5 | 77,20 | 4,70 | 4,80 | 10,35 | 97,05 |
| JIP3_LZII_#6 | 79,25 | 6,70 | 4,30 | 9,30 | 99,55 |
| JIP3_LZII_#7_1 | 34,60 | 17,50 | 18,25 | 29,65 | 100,00 |
| JIP3_LZII_#7_2 | 33,65 | 16,30 | 18,30 | 31,90 | 100,15 |
| JIP3_LZII_#8 | 77,05 | 5,15 | 4,95 | 12,95 | 100,10 |
| JIP3_LZII_#9 | 80,95 | 5,55 | 5,10 | 8,20 | 99,80 |
| JIP3_LZII_#10 | 79,10 | 6,60 | 5,65 | 9,35 | 100,70 |
| JIP3_LZII_#11 | 72,75 | 7,55 | 5,95 | 13,80 | 100,05 |